BIOCHEMISTRY
including biophysical chemistry & molecular biology

Article

pubs.acs.org/biochemistry

Molecular Dissection of *Mycobacterium tuberculosis* Integration Host Factor Reveals Novel Insights into the Mode of DNA Binding and Nucleoid Compaction

Narayanaswamy Sharadamma, Yadumurthy Harshavardhana, Apoorva Ravishankar, Praveen Anand, Nagasuma Chandra, and K. Muniyappa*

Department of Biochemistry, Indian Institute of Science, Bangalore 560012, India

ABSTRACT: The annotated whole-genome sequence of *Mycobacterium tuberculosis* indicated that Rv1388 (*Mtihf*) likely encodes a putative 20 kDa integration host factor (mIHF). However, very little is known about the functional properties of mIHF or organization of mycobacterial nucleoid. Molecular modeling of the mIHF three-dimensional structure, based on the cocrystal structure of *Streptomyces coelicolor* IHF-duplex DNA, a bona fide relative of mIHF, revealed the presence of Arg170, Arg171, and Arg173, which might be involved in DNA binding, and a conserved proline (P150) in the tight turn. The phenotypic sensitivity of *Escherichia coli* Δ*ihfA* and Δ*ihfB* strains to UV and methylmethanesulfonate could be complemented with the wild-type *Mtihf*, but not its alleles bearing mutations in the DNA-binding residues. Protein−DNA interaction assays revealed that wild-type mIHF, but not its DNA-binding variants, bind with high affinity to fragments containing *attB* and *attP* sites and curved DNA. Strikingly, the functionally important amino acid residues of mIHF and the mechanism(s) underlying its binding to DNA, DNA bending, and site-specific recombination are fundamentally different from that of *E. coli* IHF*αβ*. Furthermore, we reveal novel insights into IHF-mediated DNA compaction depending on the placement of its preferred binding sites; mIHF promotes compaction of DNA into nucleoid-like or higher-order filamentous structures. We hence propose that mIHF is a distinct member of a subfamily of proteins that serve as essential cofactors in site-specific recombination and nucleoid organization and that these findings represent a significant advance in our understanding of the role(s) of nucleoid-associated proteins.

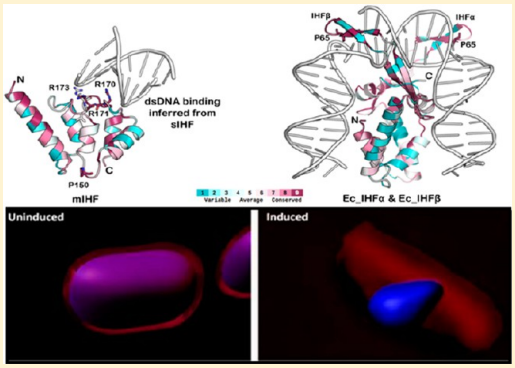

Bacterial nucleoid is a compressed helical structure composed of DNA, RNA, and small nucleoid-binding proteins, whose architecture and protein composition are regulated in a growth phase-dependent manner.[1−3] Nucleoid-associated proteins play crucial roles in many processes such as DNA replication, recombination, repair, and gene expression through DNA bending, bridging, and wrapping.[1−3] *Escherichia coli* nucleoid contains a diverse set of abundant proteins, collectively known as nucleoid-associated proteins (NAPs), which fulfill both architectural and regulatory roles.[2,3] In *E. coli*, the major NAPs include H-NS, HU, Fis, IHF, and StpA, which influence the topology of bound DNA by bending and bridging of nonadjacent DNA segments.[3] Originally discovered in *E. coli* as an essential host factor for integration/excision of phage *λ*,[4] IHF links the architecture of the genome to its function inside the cell, influencing replication[5] and transcription,[6−9] and serves as an integral component of several site-specific recombination systems.[3,10] *E. coli* IHF, a member of the DNABII structural family, is composed of two subunits, IHF*α* and IHF*β* (∼10 kDa each), each of which is required for full IHF activity.[3,8,10,11] *E. coli* IHF binds with high affinity to a 30−35 bp DNA having a conserved 3′ region with a consensus sequence of WATCAANNNNTTR (where W is A or T, R is purine, and N is any base) and a 5′ region that is degenerate but is typically AT rich.[8,10,12−14] Binding of *E. coli* IHF causes the DNA to adopt a U-turn, thus bringing the nonadjacent sequences into the proximity of each other.[12−14] However, other studies have shown that the interaction between IHF and DNA is complex, with IHF binding to DNA via different modes that induce different DNA bending patterns, and these DNA binding modes are sensitive to various solution conditions.[15,16]

Several molecular and genome-scale studies have demonstrated that the members of the IHF-HU superfamily of proteins regulate global and local gene expression in diverse species of Gram-negative and Gram-positive bacteria.[17−22] Mycobacterial IHF was originally discovered in *Mycobaterium smegmatis* as a factor essential for site-specific recombination promoted by mycobacteriophage L5 integrase (henceforth called phage L5).[23,24] Subsequently, annotation of the whole genome sequence of *Mycobaterium tuberculosis* H37Rv revealed the presence of a putative *ihf* gene in the pathogen.[25] Several lines of evidence suggest that *E. coli* NAPs share relatively low levels of amino acid identity with their counterparts in a wide variety of microorganisms, including *M. tuberculosis*.[2,3,26,27] For

Received: April 24, 2015
Revised: June 8, 2015
Published: June 12, 2015

DOI: 10.1021/acs.biochem.5b00447
Biochemistry 2015, 54, 4142−4160

example, *M. tuberculosis* H37Rv *ihf* (*Mtihf*) is predicted to encode a single 20 kDa polypeptide compared to two different protein species in *E. coli*.[25] Consequently, general features of the nucleoid structure and function described for the *E. coli* paradigm may not be relevant to other bacteria, which emphasizes the need to understand the identity and roles of NAPs, especially in pathogenic bacteria. Furthermore, unlike wild-type *E. coli* strains, IHF is essential for the growth and viability of *M. smegmatis* and *M. tuberculosis*.[24,28−30] However, despite these considerations, functional properties of *M. tuberculosis* IHF (henceforth called mIHF), the mechanism underlying the formation of higher-order nucleoprotein filaments and compaction of DNA into nucleoid, largely remain unknown.

In this study, we address two fundamental questions regarding the identity and function of mIHF. (1) Is mIHF essential for bacterial growth and DNA compaction? (2) Because mIHF is structurally unrelated to *E. coli* IHF$\alpha\beta$, what are the amino acid residues and the mechanism(s) involved in DNA binding and nucleoid compaction? Using multiple complementary methods, we show that mIHF alone was necessary and sufficient to restore genetic robustness in both *E. coli* Δ*ihfA* and Δ*ihfB* strains, induce DNA compaction, and stimulate site-specific recombination. Strikingly, our work disclosed that functionally relevant amino acid residues and the mechanism underlying binding of mIHF to DNA and site-specific recombination are different from those of *E. coli* IHF$\alpha\beta$. Overall, our data are consistent with the notion that mIHF is a distinct member of a subfamily of proteins that serve as essential cofactors in site-specific recombination and nucleoid organization and, therefore, could serve as a potential target for structure-aided drug design.

EXPERIMENTAL PROCEDURES

Homology Modeling and Sequence Alignment. The full-length protein sequence of *M. tuberculosis* IHF was retrieved from the Uniprot database (UniProtKB entry L0T6Q3).[31] The similarity of mIHF sequence with the experimentally determined protein structures in the Protein Data Bank (PDB)[32] was analyzed through BLAST[33] (http://blast.ncbi.nlm.nih.gov/Blast.cgi). Multiple-sequence alignment between different IHF proteins was obtained through the T-Coffee Web server.[34] The cocrystal structure of *Streptomyces coelicolor* IHF protein bound to dsDNA (sIHF, PDB entry 4ITQ) was the topmost hit, sharing a sequence identity of 60% (E value of 1×10^{-20}) with the C-terminal end of mIHF (residues 87−190). Consequently, sIHF protein, although lacking an N-terminal fragment of 86 amino acids, was chosen as the template for homology modeling using Modeler 9v10. The alignment between sIHF and mIHF was optimized using Promals3D.[35] The secondary structures were restrained on the basis of the boundaries derived from PSIPRED predictions.[36] The refinement of the model was iteratively conducted using KoBaMin.[37] The model with the lowest DOPE score was finally selected for analysis.[38,39]

Western Blot Analysis. Polyclonal anti-mIHF antibodies against purified mIHF were prepared in rabbits and characterized according to the standard procedures.[40] To investigate the identity of intracellular IHF, *M. tuberculosis* H37Rv cells were cultured in Middlebrook 7H9 medium (Difco) supplemented with 10% (v/v) albumin/dextrose/catalase enrichment and 0.05% (v/v) Tween 80 in a shaker incubator with a speed of 180 rpm at 37 °C.[41] Whole-cell lysates were prepared as previously described.[42] Briefly, cells equivalent to 1.0 at A_{600} at different time points of growth were resuspended in SDS loading buffer and disrupted by sonication using an ultrasonic liquid processor (MISONIX) two or three times for 30−40 s in pulse mode at 21% amplitude. The whole-cell lysates were treated with DNase I (1 μg/mL) and RNase A (0.2 μg/mL), prior to Western blot analysis. Equal amounts of protein from the lysates were separated by SDS−PAGE and transferred onto a nitrocellulose membrane. The blot was blocked for 2 h at 24 °C with 1% bovine serum albumin in phosphate-buffered saline. The blot was washed and probed in a solution containing 10 mM sodium phosphate (pH 7.4) and 150 mM NaCl with 0.1% bovine serum albumin, 0.1% ovalbumin, 0.1% Tween 20, and 0.02% sodium azide, and anti-mIHF or anti-SigA antibodies for 12 h at 4 °C. The blot was subsequently washed three times with PBS and incubated for 1 h at room temperature with alkaline phosphatase- or peroxidase-conjugated (Sigma-Aldrich, St. Louis, MO) secondary antibody. Finally, the blot was developed with the Fast 5-bromo-4-chloro-3-indolyl phosphate−nitroblue tetrazolium kit (Sigma-Aldrich) or enhanced chemiluminescence (ECL).

MMS and UV Sensitivity Assays. An *E. coli* wild-type, Δ*ihfA*, or Δ*ihfB* strain harboring p*Mtihf* was grown in LB broth supplemented with 100 μg/mL ampicillin. At an A_{600} of 0.4, cells were then treated with 0.5% methylmethanesulfonate (MMS) for 45 min. Cells were collected by centrifugation and resuspended in an equal volume of a solution containing M9 salts. The indicated dilutions were made in M9 salts and spotted on LB plates supplemented with 100 μg/mL ampicillin. In parallel, plates containing serial dilutions of cells were UV irradiated using an ultraviolet lamp (UVGL-58, 254 nm, G6T5 lamp). Plates were incubated at 37 °C in the dark for 22 h.

Preparation of DNA Substrates. Plasmids pMH57 (*attB*) and pSS19 (*attP*) were linearized by restriction digestion with HindIII and BamHI, respectively.[40] DNA fragments were labeled at the 5′-end using [γ-^{32}P]ATP and T4 polynucleotide kinase (New England Biolabs). Subsequently, labeled DNA was cleaved with EcoRI to release 600 and 546 bp fragments, respectively. The cleaved DNA fragments were electrophoresed through a 5% polyacrylamide gel in 45 mM Tris-borate buffer (pH 8.3) containing 1 mM EDTA at 10 V/cm for 8 h. The bands were excised from the gel, eluted into TE buffer [10 mM Tris-HCl (pH 7.5) and 1 mM EDTA].

Curved DNA and 230 bp (pB16) and 220 bp noncurved DNA (pNB10) were excised from the pB16 and pNB10 plasmids,[43] respectively, by digestion with HindIII and EcoRI. DNA fragments were labeled at the 5′-end using [γ-^{32}P]ATP and T4 polynucleotide kinase. The labeled DNA was electrophoresed through a 8% polyacrylamide gel in 45 mM Tris-borate buffer (pH 8.3) containing 1 mM EDTA at 10 V/cm for 6 h as described previously.[40] The bands corresponding to 230 and 220 bp were excised from the gel and eluted into TE buffer [10 mM Tris-HCl (pH 7.5) and 1 mM EDTA].

Isolation of the *M. tuberculosis ihf* Gene. The coding sequence corresponding to the *M. tuberculosis* H37Rv *ihf* gene (Rv1388) was amplified via polymerase chain reaction (PCR) from the cosmid DNA (MYTC21B4) using the following ODNs (forward primer, 5′-GAGGGCCATATGTTAGGCAA-CACTATTCATG-3′; and reverse primer, 5′-ATACATGGA-TCCTTAGGCGGAGCCGAA-3′) carrying the sites for NdeI and BamHI, respectively. PCR amplification yielded a product of the predicted length (573 bp). The PCR product was gel purified and digested with restriction enzymes. By using

DOI: 10.1021/acs.biochem.5b00447
Biochemistry 2015, 54, 4142−4160

Table 1. Primer Sequences Used To Generate mIHF Protein Variants

mutant	primer	sequence
R170A/R171A	forward	5′-GCTGGAAATTGCGCCCACCGCCGCCCTTCGTGGCCTCGGTGACCG-3′
R170A/R171A	reverse	5′-CGGTCACCGAGGCCACGAAGGGCGGCGGTGGGCGCAATTTCCAGC-3′
R173A	forward	5′-GCCCACCGCCGCCCTTGCTGGCCTCGGTGACCGTCAGC-3′
R173A	reverse	5′-GCTGACGGTCACCGAGGCCAGCAAGGGCGGCGGTGGGC-3′
P150A	forward	5′-CGCTGCTTGAGGCCTTGGCAAAGGTGGGCAAGGTC-3′
P150A	reverse	5′-GACCTTGCCCACCTTTGCCAAGGCCTCAAGCAGCG-3′

terminal NdeI and BamHI restriction sites that were incorporated into the DNA during amplification, the fragment was directionally ligated into NdeI and BamHI sites of *E. coli* expression vector pET15b. The resultant plasmid was designated p*Mtihf*. The identity of the recombinant plasmid was ascertained by restriction analysis and DNA sequencing. To confirm the identity of the protein encoded by *Mtihf*, we raised antibodies against purified mIHF and characterized them according to the standard procedures.[40]

Construction of *M. tuberculosis* Mutant *ihf* Expression Plasmids. PCR primers used for site-directed mutagenesis are listed in Table 1. Plasmid p*Mtihf* was mutated using the QuikChange method with PfuTurbo DNA polymerase and DpnI. The arginine at position 170, 171, or 173 was replaced with alanine or aspartate. Similarly, proline at position 150 was substituted with alanine. *E. coli* DH5α was used for plasmid amplification. The mutations were ascertained by restriction analysis and DNA sequencing.

Expression and Purification of *M. tuberculosis* IHF Wild-Type and Mutant Proteins. A culture of *E. coli* Rosetta2 (DE3)pLysS strain harboring plasmid p*Mtihf* was grown in Luria-Bertani broth containing 100 μg/mL ampicillin and 34 μg/mL chloramphenicol at 37 °C until the A_{600} reached 0.5. mIHF was induced by the addition of isopropyl 1-thio-β-D-galactopyranoside (IPTG) to a final concentration of 0.5 mM. The culture was incubated while being gently shaken at 37 °C for 6 h. Cells were collected by centrifugation, washed in STE buffer [10 mM Tris-HCl (pH 8), 100 mM NaCl, and 1 mM EDTA], resuspended in buffer A [10 mM Tris-HCl (pH 8), 150 mM NaCl, and 10% (v/v) glycerol], and stored at −80 °C. Cells were thawed and lysed by sonication (Ultrasonic Processor, model GEX-750) in a pulse mode on ice at 60% duty cycles. The suspension was centrifuged in a Beckman Ti-45 rotor at 30000 rpm for 1 h at 4 °C. The supernatant was then loaded onto a Ni^{2+}-NTA agarose column equilibrated with buffer A. mIHF was eluted with a 30 to 500 mM linear gradient of imidazole in buffer A. Peak fractions were pooled and dialyzed against buffer B [10 mM Tris-HCl (pH 7.5), 1 mM EDTA, 1 mM DTT, 100 mM NaCl, and 10% (v/v) glycerol]. The dialyzed sample was loaded onto a double-stranded DNA-cellulose column that had been previously equilibrated with buffer B. IHF was eluted with a 0.1 to 1 M linear gradient of NaCl in buffer B. Peak fractions were pooled and dialyzed against buffer C [10 mM Tris-HCl (pH 7.5), 1 mM EDTA, 1 mM DTT, 150 mM NaCl, and 20% (v/v) glycerol]. The purity of IHF was assessed by SDS−PAGE and found to be >98%. Aliquots of mIHF were stored at −80 °C.

M. tuberculosis IHF protein variants, i.e., single-point (P150A) and triple-point (R170A/R171A/R173A and R170D/R171D/R173D) mutant proteins were expressed in the *E. coli* Rosetta2 (DE3)pLysS strain. Cells were grown in LB broth containing 100 μg/mL ampicillin and 34 μg/mL chloramphenicol at 37 °C until the A_{600} reached 0.5. Mutant proteins were induced by the addition of IPTG to a final concentration of 0.5 mM. The culture was incubated while being gently shaken at 37 °C for 6 h. Cells were collected by centrifugation, washed in STE buffer [10 mM Tris-HCl (pH 8), 100 mM NaCl, and 1 mM EDTA], resuspended in buffer A [10 mM Tris-HCl (pH 8.0), 150 mM NaCl, and 10% (v/v) glycerol], and stored at −80 °C. Cells were thawed and lysed by sonication (model GEX-750, Ultrasonic Processor) on ice at 60% duty cycles in a pulse mode. The suspension was centrifuged in a Beckman Ti-45 rotor at 30000 rpm for 1 h at 4 °C. The supernatant was then loaded onto a Ni-NTA column equilibrated with buffer A. IHF was eluted with a 30 to 500 mM linear gradient of imidazole in buffer A. Peak fractions were pooled and dialyzed against buffer B [10 mM Tris-HCl (pH 7.5), 1 mM EDTA, 1 mM DTT, 150 mM NaCl, and 20% (v/v) glycerol]. The purity of IHF mutant proteins was assessed by SDS−PAGE and found to be >98%. Aliquots of mIHF variants were stored at −80 °C.

Expression and Purification *E. coli* IHF$\alpha\beta$. *E. coli* IHF$\alpha\beta$ was purified as previously described.[44] Plasmid pET21a IHF, harboring *E. coli ihfA* and *ihfB*, was purchased from Addgene (Cambridge, MA) and transformed into the *E. coli* Rosetta2-(DE3)pLysS strain. Bacteria were grown in LB broth containing ampicillin (100 μg/mL) and chloramphenicol (34 μg/mL) at 37 °C until the A_{600} reached 0.6 and induced by the addition of 1 mM IPTG. The culture was incubated while being gently shaken at 37 °C for 6 h. Cells were collected by centrifugation and washed in STE buffer [10 mM Tris-HCl (pH 8), 100 mM NaCl, and 1 mM EDTA] and resuspended in lysis buffer [100 mM Tris-HCl (pH 8.0), 1 mM EDTA, 10% sucrose, 10% glycerol, and 1 M NaCl] supplemented with 1 mM PMSF. Cells were lysed by sonication (model GEX-750, ultrasonic processor) on ice at 60% duty cycles in a pulse mode. The suspension was centrifuged in a Beckman Ti-45 rotor at 30000 rpm for 1 h at 4 °C. To the supernatant was added solid $(NH_4)_2SO_4$ to 50% saturation at 4 °C, and the precipitate was removed by centrifugation. To the supernatant was added $(NH_4)_2SO_4$ to 80% saturation at 4 °C, and the precipitated proteins were recovered by centrifugation. The precipitate was resuspended and dialyzed overnight against buffer A (25 mM HEPES, 0.1 mM EDTA, 5% glycerol, and 100 mM NaCl) at 4 °C. The dialysate was then loaded onto a heparin-Sepharose column that had been previously equilibrated with buffer A. IHF$\alpha\beta$ was eluted with a 400 mM to 1.6 M linear gradient of NaCl in buffer A. The peak fractions were pooled and dialyzed against storage buffer B (25 mM HEPES, 0.1 mM EDTA, 10% glycerol, and 100 mM NaCl). The purity of IHF$\alpha\beta$ was assessed by SDS−PAGE and found to be >98% pure. Aliquots of *E. coli* IHF$\alpha\beta$ were stored at −80 °C.

Microscopy. The *E. coli* Δ*ihfA* strain, harboring Mt*ihf* or its variants, was grown in LB broth at 37 °C to an A_{600} of 0.4. mIHF expression was induced with 0.8 mM IPTG for 2 h at 37 °C. The cells from the IPTG-induced and uninduced culture

DOI: 10.1021/acs.biochem.5b00447
Biochemistry 2015, 54, 4142−4160

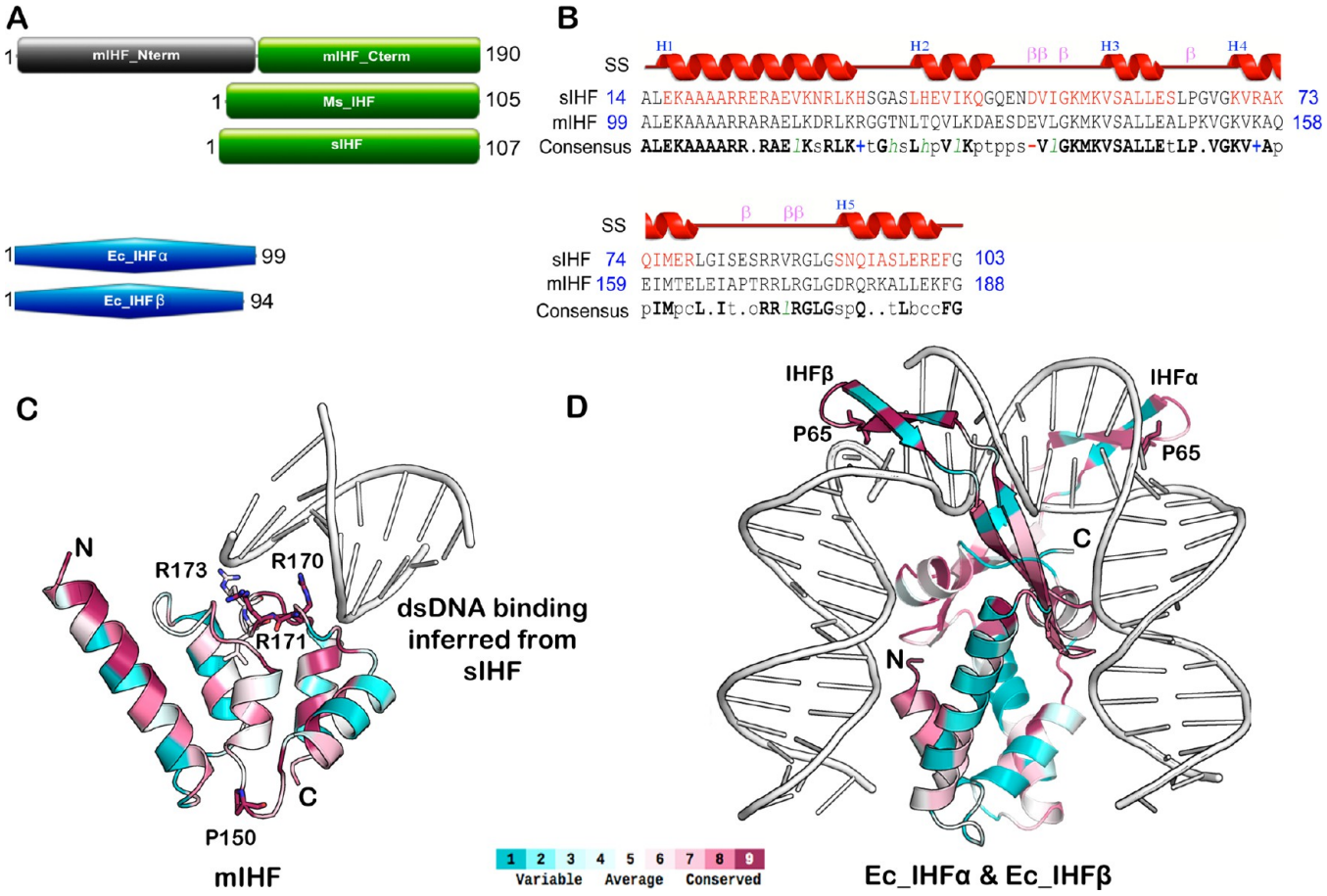

Figure 1. (A) Domain architecture of IHFs from *M. tuberculosis* (mIHF), *M. smegmatis* (Ms_IHF), *S. coelicolor* (sIHF), and *E. coli* (Ec_IHFα and Ec_IHFβ). (B) Sequence alignment between sIHF and mIHF derived from PROMALS3D. The assigned secondary structures are displayed above the alignment. The coiled-coil structures (H1−H5) represent α-helical bundles and the lines β-sheets and turns. (C) Homology-modeled three-dimensional structure of the mIHF−dsDNA complex, using the crystal structure of the sIHF−dsDNA complex as a template (PDB entry 4ITQ).[48] The mIHF DNA (depicted as a white cartoon)-binding residues have been inferred from the superposition of the sIHF−dsDNA cocrystal structure onto the mIHF−dsDNA modeled structure. The residues (R171, R170, and R173) implicated in DNA binding are depicted as sticks. (D) Structure of *E. coli* IHF$\alpha\beta$ complexed with dsDNA (PDB entry 1IHF).[14] Both structures were colored on the basis of the conservation of residues derived from the Consurf database.[38]

were collected by centrifugation, washed twice with PBS, and then fixed with 70% ethanol. Cells were incubated for 15 min at room temperature and washed twice in PBS. Cells were spread evenly on a poly-L-lysine-coated glass slide and air-dried for 20 min, followed by treatment with a DAPI solution (5 ng/μL) for 2 min at room temperature in the dark. Slides were gently washed with PBS to remove an excess of DAPI solution, air-dried, and mounted in ProLong Gold Antifade reagent (Life technologies). Cells were then visualized using an LSM-710 (Zeiss) confocal laser scanning microscope with a 63× oil objective. Z-Stacks were collected at intervals of 3−4 s. Three-dimensional reconstructions were conducted by weighted back projection of aligned images. Tomographic reconstructions thus obtained were processed as described previously.[45]

Gel Mobility Shift Assay. Reaction mixtures (20 μL) contained 40 mM Tris-HCl (pH 8), 100 mM KCl, 1 mM dithiothreitol (DTT), 5 mM potassium phosphate, 5% glycerol, 0.5 mM EDTA, with 2 nM ^{32}P-labeled double-stranded DNA (dsDNA), and the indicated amounts of mIHF or *E. coli* IHF$\alpha\beta$ as specified in the figure legends. After incubation at 37 °C for 20 min, 2 μL of 10% loading dye was added to each sample. Samples were electrophoresed through polyacrylamide gels as follows: in the case of mIHF, a 6% gel, run at 12 V/cm for 6 h; in the case of *E. coli* IHF$\alpha\beta$, a 4% gel run at 10 V/cm for 4 h; for pB16 and pNB10 DNA, in 0.5× TAE [20 mM Tris-acetate buffer (pH 7.4)] containing 0.5 mM EDTA at 4 °C. Gels were dried and the bands visualized and quantified as previously described.[26]

***In Vitro* Recombination Assay.** The assay was performed as described previously.[46] Phage L5 integrase was purified as previously described.[46] Reaction mixtures contained 20 mM Tris-HCl (pH 7.5), 1 mM DTT, 25 mM NaCl, 5 mM spermidine, 0.5 μg of phage L5 integrase, 200 ng of negatively superhelical pMH39 DNA (contains the *attP* site), 200 ng of 3.9 kb linear dsDNA containing the *attB* site (generated by digestion of pMH57 with *Hin*dIII), and increasing concentrations (0.05−2.5 μg) of mIHF or the Arg-Ala triple mutant protein. After incubation for 3 h at 24 °C, the reaction was terminated by the addition of 1.2 μL of a solution containing 5 mM EDTA, 0.1% SDS, and 0.4 mg/mL proteinase K. Samples were incubated for 5 min at 24 °C and electrophoresed through a 0.8% agarose gel at 35 V for 10 h. Gels were stained with ethidium bromide and the products identified following visualization under UV light.

DNA Circularization Assay. The assay was performed as previously described.[47] Reaction mixtures (20 μL) contained 20

DOI: 10.1021/acs.biochem.5b00447
Biochemistry 2015, 54, 4142−4160

mM Tris-HCl (pH 8.0), 150 mM KCl, 1 mM DTT, 1 mM potassium phosphate, 5% glycerol, 0.25 nM ^{32}P-labeled 140 bp duplex DNA (derived from digestion of pUC19 plasmid DNA with TfiI), and the indicated concentrations of either mIHF or *E. coli* IHF$\alpha\beta$. After incubation at 37 °C for 30 min, 20 units of T4 DNA ligase (Fermentas) and 1× ligase buffer was added, and incubation was extended for 30 min. In reactions involving Exo III, samples were further incubated at 37 °C for 20 min with 5 units of Exo III. The reaction was terminated by the addition of 1 μL of 20% SDS and 1 μL of 10 mg/mL proteinase K, followed by incubation at 37 °C for 20 min. DNA was extracted with a phenol/chloroform solution and precipitated with ethanol. The DNA pellet, obtained after centrifugation, was resuspended in 5 μL of 6× DNA gel loading buffer. Samples were subjected to electrophoresis through a 5% polyacrylamide gel in 45 mM Tris-borate buffer (pH 8.3) containing 1 mM EDTA at 10 V/cm for 5 h. The gels were dried, and the bands were visualized using a Fuji FLA-9000 phosphorimager.

Atomic Force Microscopy. AFM experiments were performed as previously described.[47] DNA fragments were prepared by digestion of closed circular DNA (pB16 and pNB10) with ScaI or HindIII.[34] Reaction mixtures contained 20 mM Tris-HCl (pH 7.5), 2 mM $MgCl_2$, 150 mM KCl, 5 ng of the indicated DNA, and 50 nM IHF (Figure 6B) or 200 nM IHF (Figure 6C). After incubation for 30 min, 5 μL aliquots were applied to the surface of freshly cleaved mica. Images were acquired using an SNL (silicon tip on nitride lever) AFM probe (Agilent Technologies, force constant of 21−98 N/m) and an Agilent AFM controller operated in tapping mode in air. Imaging was conducted at a resolution of 512 × 512 pixels. Raw data were selected with the Picoimage software, and the same was used to "flatten" AFM images with second-order polynomial fitting.

RESULTS

Sequence Alignments, Homology Modeling, and Identification of Candidate Residues for Mutagenesis. The annotated whole-genome sequence of *M. tuberculosis* H37Rv identified Rv1388 as the *ihf* gene (www.sanger.ac.uk/Projects/M_tuberculosis). Multiple-sequence alignment of the deduced amino acid sequence of Rv1388 revealed the presence of 86 additional amino acids at the N-terminus of mIHF, but not in *M. smegmatis* IHF (Figure 1A). A pairwise BLAST search of the PDB indicated that mIHF shows 60% sequence identity with *S. coelicolor* (sIHF).[48] Figure 1B shows the sequence alignment between sIHF and mIHF derived from PROMALS3D.[35] To generate the mIHF homology model, the crystal structure of sIHF, determined at a resolution of 2.7 Å in complex with double-stranded DNA (PDB entry 4ITQ), was used as a template,[48] and the homology model was determined using MODELER.[34] Figure 1C shows the mIHF structure in complex with duplex DNA colored on the basis of the conservation of amino acid residues derived from alignment with unique protein entries of Uniprot using ConSurf.[49] Superposition of the backbone traces of the homology-modeled mIHF structure with the sIHF cocrystal structure yielded a low root-mean-square deviation value of 0.27 Å, indicating a good match between the two proteins. The DNA-binding site was inferred from superposition of the crystal structure of sIHF complexed with double-stranded DNA (dsDNA) onto the modeled structure of the mIHF−dsDNA complex. These studies predicted an ensemble of residues in mIHF, Arg170, Arg171, and Arg173, corresponding to Arg85, Arg86, and Arg88 residues in sIHF that might be involved in DNA binding activity.[48] Comparison between the mIHF−dsDNA homology model and the crystal structure of *E. coli* IHF$\alpha\beta$ with dsDNA revealed significant differences (Figure 1D). The central structural element in *E. coli* IHF$\alpha\beta$ is a pair of β-ribbon arms each with a critical Pro65 residue that gets inserted into the minor groove at the high-affinity binding site. Additionally, IHF contacts dsDNA via the phosphodiester backbone and the dsDNA wrapped around the protein and bent by >160°.[8,14] In mIHF, Pro150 is the corresponding conserved residue that is embedded in a tight turn (Figure 1C). Because it is not in contact with DNA, it is possible that it could be involved in maintaining the tertiary structure of mIHF.

Expression Patterns of *M. tuberculosis* IHF at Various Growth Phases. To assess whether the intracellular levels of mIHF change during different stages of growth under *in vitro* conditions, *M. tuberculosis* H37Rv was grown in Middlebrook 7H9 liquid medium supplemented with 10% (v/v) albumin/dextrose/catalase enrichment and 0.05% (v/v) Tween 80 as described in Experimental Procedures. Growth was monitored by measuring the optical density of cells at 600 nm (Figure 2A).

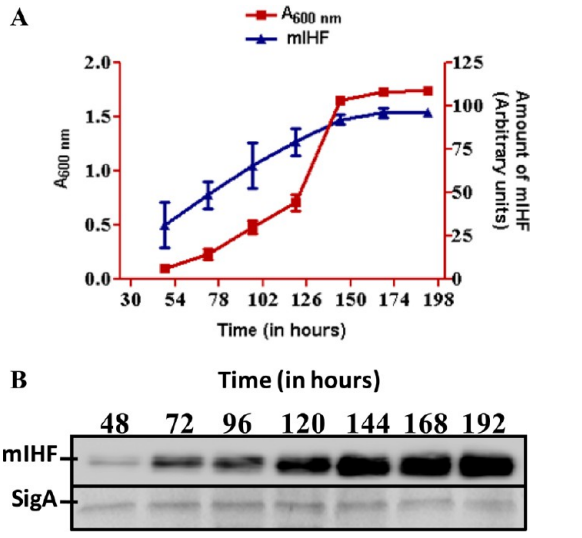

Figure 2. Growth phase-dependent expression of IHF of *M. tuberculosis*. (A) At the indicated time points of *M. tuberculosis* H37Rv growth, cells were harvested and whole-cell lysates were prepared. Fifty micrograms of protein from whole-cell lysates at each time point of growth was separated by SDS−PAGE and transferred onto the nitrocellulose membrane. The blots were probed with anti-mIHF- or Sig-specific antibodies (panels A and B, respectively) followed by secondary antibodies. Protein signals were visualized following Western blotting as described in Experimental Procedures. SigA protein served as an internal loading control. Arbitrary units represent relative mean expression levels of mIHF and SigA over different growth phases and times.

The growth transition from exponential to stationary phase began after ~140 h. To determine the levels of IHF, whole-cell lysates from cells harvested at different time points during the growth cycle were subjected to Western blot analysis using anti-mIHF-specific antibodies (Figure 2B). In the early phases of exponential growth, the level of mIHF was low; however, its abundance steadily increased by ~4-fold when the cells reached the stationary phase of growth (Figure 2A). Our results are in agreement with previously published data on the intracellular

DOI: 10.1021/acs.biochem.5b00447
Biochemistry 2015, 54, 4142−4160

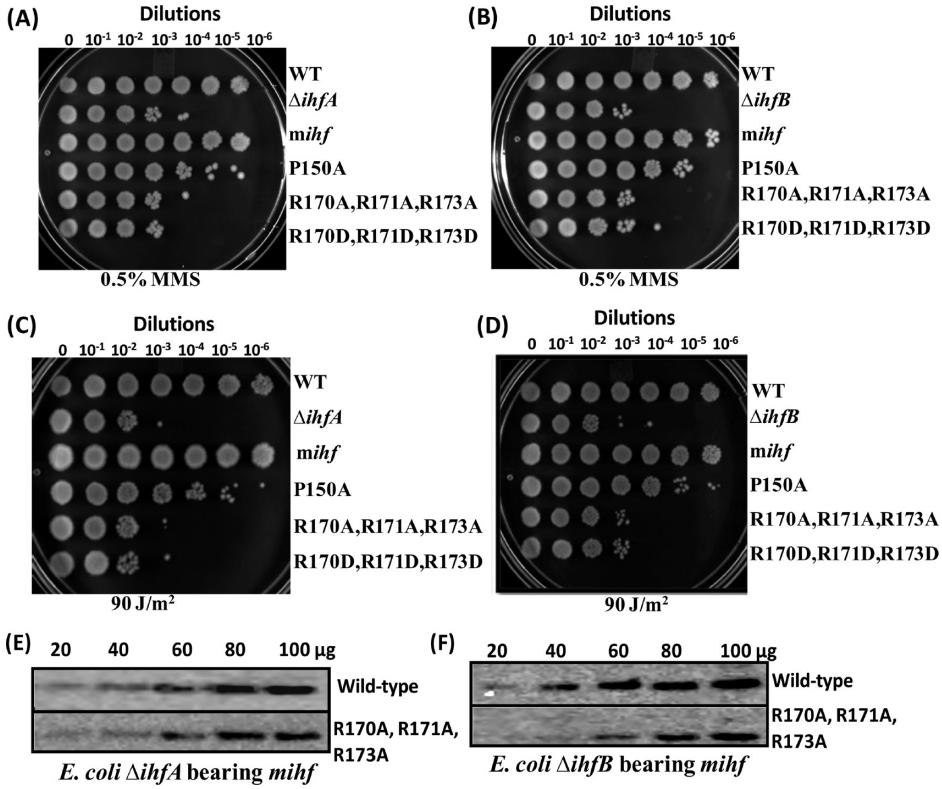

Figure 3. *M. tuberculosis ihf* complements ultraviolet radiation (UV) and methylmethanesulfonate (MMS) sensitivity of *E. coli* Δ*ihfA* and Δ*ihfB* strains. (A and B) Wild-type *Mtihf* but not its mutant alleles provides resistance to MMS toxicity in *E. coli* Δ*ihfA* and Δ*ihfB* strains. (C and D) Wild-type *Mtihf* but not its mutant alleles rescues UV radiation sensitivity in *E. coli* Δ*ihfA* and Δ*ihfB* strains. Expression of *Mtihf* in *E. coli* Δ*ihfA* (E) and Δ*ihfB* (F) strains. Increasing amounts of protein from whole-cell lysates (20, 40, 60, 80, and 100 μg) from exponentially growing cells (at A_{600} = 1.5) were separated via SDS−PAGE and transferred onto the nitrocellulose membrane. The membrane was probed using the anti-mIHF antibody and visualized as described in Experimental Procedures.

concentration of *E. coli* IHF$\alpha\beta$, which varies from 12000 molecules in the exponential growth phase to 55000 molecules (~4-fold) in the stationary phase.[50] Western blot analysis of *M. tuberculosis* SigA, which served as a loading control,[51] did not reveal any significant changes in its levels during the bacterial growth cycle. The N-terminal amino acid sequence of the first 10 amino acids of mIHF indicated that indeed it has 86 additional amino acid residues (data not shown).

***M. tuberculosis ihf* Is Necessary and Sufficient To Maintain Viability of *E. coli* Δ*ihfA* and Δ*ihfB* Strains against Genotoxic Stress.** It is known that mutations in *ihfA* or *ihfB* in *E. coli* or *Salmonella typhimurium* generate a phenotype similar to that of the double mutant,[18,20] and *ihfA* is essential for *E. coli* growth and efficient colonization.[11,52−54] However, exactly how IHF contributes to viability has not been defined. Investigating the functionality of *ihf* in *M. smegmatis* and *M. tuberculosis* mutants is difficult because it is essential for cell viability.[24,28−30] To explore the connection between mIHF and cell viability, we investigated the ability of *M. tuberculosis ihf* to complement the *E. coli* Δ*ihfA* or Δ*ihfB* strain for growth and against genotoxic stress. Toward this end, we chose methylmethanesulfonate (MMS) and UV light (UV), which are widely used genotoxins in DNA recombinational repair/replication studies that impact the genome via different mechanisms. MMS methylates N7-deoxyguanosine and N3-deoxyadenosine, and to a much lesser extent other oxygen and nitrogen atoms in DNA bases, and also methylates the phosphodiester linkage leading to double-stranded DNA breaks and stalling of replication forks. On the other hand, UV radiation involves helix-distorting lesions such as bipyrimidine UV photoproducts. We used *E. coli* expression vectors in pET15b containing full-length *M. tuberculosis ihf* under the control of the T7 promoter. We also constructed similar plasmids in pET15b carrying *Mtihf* variants bearing triple-point mutations in which R170, R171, and R173 residues were replaced with Ala or Asp, predicted to be involved in DNA binding, and a plasmid-bearing point mutation in which P150 was substituted with Ala (see Figure 1C). Serial dilutions of the indicated wild-type, mutant, and complemented mutant strains treated with either UV light or MMS were spread on LB agar plates and incubated as described in Experimental Procedures. Wild-type *E. coli ihfA* and *ihfB* strains showed slight or no sensitivity to the indicated doses of MMS or UV radiation (Figure 3A−D). On the other hand, Δ*ihfA* or Δ*ihfB* strains exhibited greater sensitivity at the indicated doses of UV radiation and MMS. In contrast, the growth of Δ*ihfA* and Δ*ihfB* strains harboring *Mtihf* was nearly comparable to that of the wild-type strains, indicating protection against genotoxicity caused by UV and MMS (Figure 3A−D). Interestingly, the mIHF Arg-Ala triple mutant (R170A/R171A/R173A) was relatively more sensitive to MMS and UV radiation than *Mtihf* P150A in both Δ*ihfA* and Δ*ihfB* strains (Figure 3A−D). Similar results were observed with the mIHF Arg-Asp (R170D/R171D/R173D) triple mutant in both Δ*ihfA* and Δ*ihfB* strains (Figure 3A−D). Immunoblot analyses indicated the presence of nearly equivalent amounts of wild-type and Arg-Ala triple mutant (R170A/R171A/R173A) mIHF proteins in both Δ*ihfA* and Δ*ihfB* strains (Figure 3E,F). These results indicate that the

DOI: 10.1021/acs.biochem.5b00447
Biochemistry 2015, 54, 4142−4160

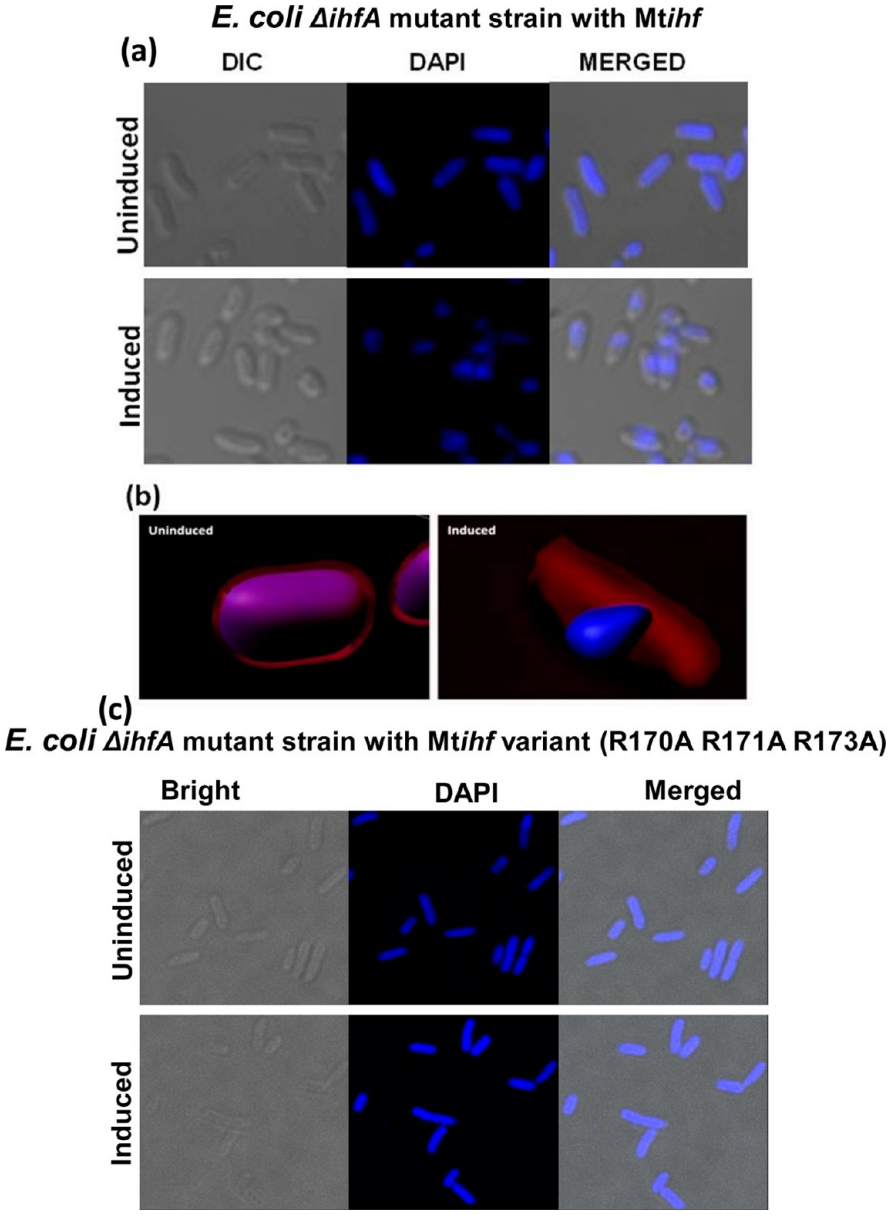

Figure 4. mIHF induces nucleoid compaction. (a) Confocal laser scanning microscopy images of DAPI-stained *E. coli* Δ*ihfA* cells harboring *Mtihf* from uninduced and 0.8 mM IPTG-induced cultures. Representative pictures depict differential interference contrast (DIC), DAPI-stained, and merged images. The scale bar is 2 μm for all panels. (b) Representative pictures depicting the 3D reconstructed images of uninduced (left) and IPTG-induced (right) *E. coli* harboring *Mtihf*. Nucleoid stained with DAPI is colored blue, and the false-red color corresponds to cell body. (c) Confocal laser scanning microscopy images of DAPI-stained *E. coli* Δ*ihfA* cells harboring the *Mtihf* triple mutant (R170A/R171A/R173A) from uninduced and 0.8 mM IPTG-induced cultures. The scale bar is 2 μm for all panels.

lack of complementation by the *Mtihf* Arg-Ala triple mutant was not due to the absence of mIHF. Similar results were also seen with the expression of *Mtihf* Arg-Asp triple mutant and P150A proteins (data not shown). Furthermore, all the mutant proteins were stable in *E. coli,* so that they could be purified in large amounts for biochemical and functional analyses (see below). Altogether, the data indicate that *Mtihf* alone is necessary and sufficient to restore viability to both Δ*ihfA* and Δ*ihfB* strains against genotoxic stress.

***M. tuberculosis* IHF Induces Compaction of DNA into Nucleoids.** The foregoing results suggest that *Mtihf* helps *E. coli* to overcome the effects of genotoxic stress. We therefore sought to visualize the nucleoid morphologies of DAPI (4′,6-diamidino-2-phenylindole)-stained *E. coli* cells bearing *Mtihf* under uninduced and isopropyl β-D-thiogalactopyranoside (IPTG)-induced conditions using confocal laser scanning microscopy. Analyses of uninduced *E. coli* Δ*ihfA* cells showed light diffusion and even staining throughout the cytoplasm (98%; n = 60) (Figure 4a, top panel). In induced *E. coli* Δ*ihfA* cells (>90%; n = 50), we observed a single and highly condensed nucleoid structure in a small volume of the cell (Figure 4a, bottom panel). Furthermore, three-dimensional (3D) imaging of *E. coli* Δ*ihfA* cells revealed highly compact nucleoid structures with a well-defined shape in induced but not in uninduced cells (Figure 4b), consistent with the idea that mIHF is a component of *E. coli* nucleoid and plays a role in the compaction of DNA into nucleoids. The expression of the *Mtihf* variant (R170A/R171A/R173A) from the same plasmid

DOI: 10.1021/acs.biochem.5b00447
Biochemistry 2015, 54, 4142−4160

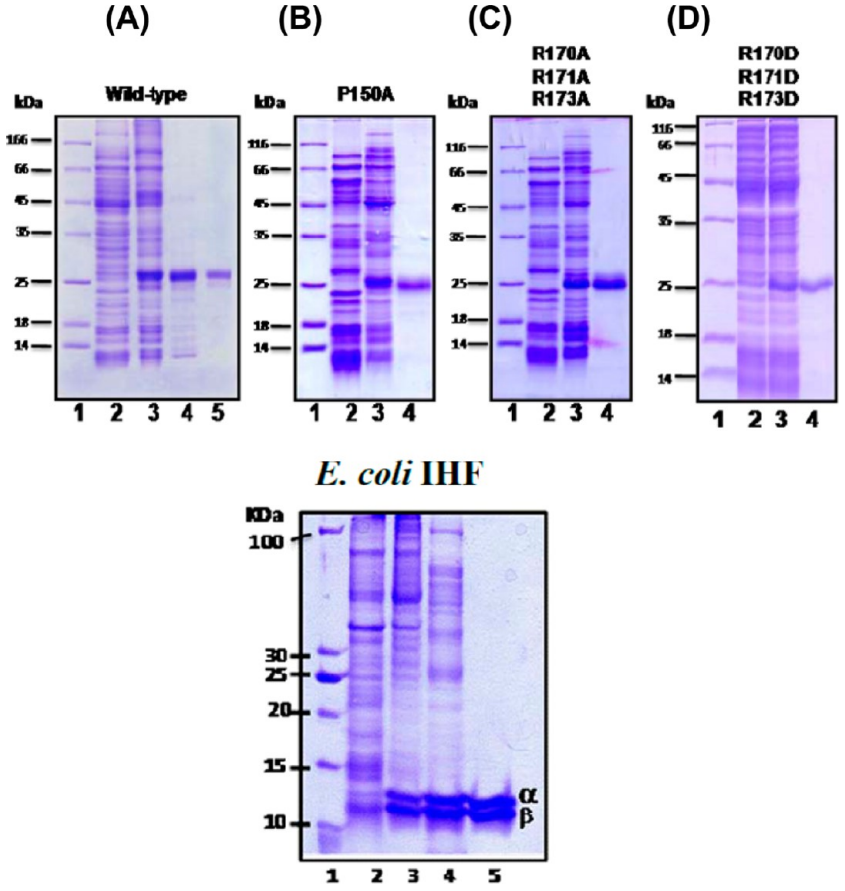

Figure 5. Purification of *M. tuberculosis* and *E. coli* IHF proteins. (A) SDS−PAGE analysis showing expression and purification of wild-type mIHF from *E. coli*. Ten micrograms (lanes 2 and 3), 3 μg (lane 4), or 1 μg (lane 5) of protein from the indicated samples (see below) was resolved by SDS−PAGE and visualized by staining with Coomassie blue: lane 1, protein molecular weight markers; lane 2, sample from uninduced whole-cell lysate; lane 3, sample from induced whole-cell lysate; lane 4, chromatography on Ni^{2+}-NTA agarose; lane 5, chromatography on double-stranded DNA. (B−D) Expression and purification of mIHF variants. Protein samples were separated by SDS−PAGE and visualized by staining with Coomassie blue: lane 1, protein molecular weight markers; lane 2, sample form uninduced whole-cell lysate (10 μg); lane 3, sample from induced whole-cell lysate (3 μg); lane 4, chromatography on Ni^{2+}-NTA agarose (1 μg). The bottom panel shows the analysis of the expression and purification of *E. coli* IHF$\alpha\beta$ by SDS−PAGE. Ten micrograms (lanes 2−4) or 3 μg (lane 5) of protein from the indicated step of the purification scheme was separated by SDS−PAGE and visualized by staining with Coomassie blue: lane 1, protein molecular weight markers; lane 2, sample from uninduced whole-cell lysate; lane 3, sample from induced whole-cell lysate; lane 4, 80% $(NH_4)_2SO_4$ pellet fraction; lane 5, chromatography on heparin-Sepharose.

and promoter in *E. coli* Δ*ihfA* cells failed to induce nucleoid compaction (>94%; n = 65) (Figure 4c). Immunoblot analysis of whole-cell lysates from *E. coli* Δ*ihfA* cells expressing *Mtihf* and its triple mutant showed that they were expressed at similar levels (Figure 3E). These data clearly establish a direct role for wild-type *Mtihf* in nucleoid organization.

The Ability To Interact with *attB* and *attP* Sites Is Conserved between *M. tuberculosis* and *E. coli* IHF. The observation that the site-specific mutants failed to complement the UV and MMS sensitivity phenotypes of *E. coli* Δ*ihfA* and Δ*ihfB* strains led us to explore the mechanistic basis for their defects. Scrutinizing the sequence identity between *M. tuberculosis* and *E. coli* IHF proteins seemed insufficient, *a priori*, to infer the DNA binding specificity of mIHF. Accordingly, we cloned, expressed, and purified wild-type and variant forms of mIHF and *E. coli* IHF$\alpha\beta$ (Figure 5). To investigate the DNA binding properties of mIHF, we chose dsDNA containing phage L5 *attB* (600 bp) or *attP* (546 bp) sites.[24,55] Binding reactions were performed with 2 nM ^{32}P-labeled dsDNA having an *attP* or *attB* site and increasing concentrations of mIHF. Reaction mixtures were subjected to an electrophoretic mobility shift assay (EMSA) as described in Experimental Procedures. The gel shift assays indicated that mIHF altered the mobility of dsDNA. As shown in panels A and B of Figure 6, mIHF bound to *attB*- and *attP*-containing dsDNA to form stable complexes. However, mIHF at lower concentrations formed poorly resolved complexes, thus generating a smear (Figure 6A, lanes 3 and 4, and Figure 6B, lanes 4 and 5). With increasing mIHF concentrations, the intensity of the slower-moving band gradually increased, resulting in the formation of a well-defined band, indicating that saturation had been achieved (Figure 6A, lanes 5−10, and Figure 6B, lanes 8−10). However, mIHF bound more efficiently to the *attB* site-containing substrate than to the *attP* site-containing substrate. We next tested the effect of mutations in amino acid residues of mIHF that are predicted to make direct contacts with DNA. We observed that substitution of Ala or Asp for R170, R171, and R173 as well as Ala for P150 completely abolished binding of mIHF to *attB*- and *attP*-containing dsDNA substrates as assessed by an EMSA (Figure 6C−H). Quantitative analysis of the extent of complex formation between mIHF and various DNA substrates, as a

DOI: 10.1021/acs.biochem.5b00447
Biochemistry 2015, 54, 4142−4160

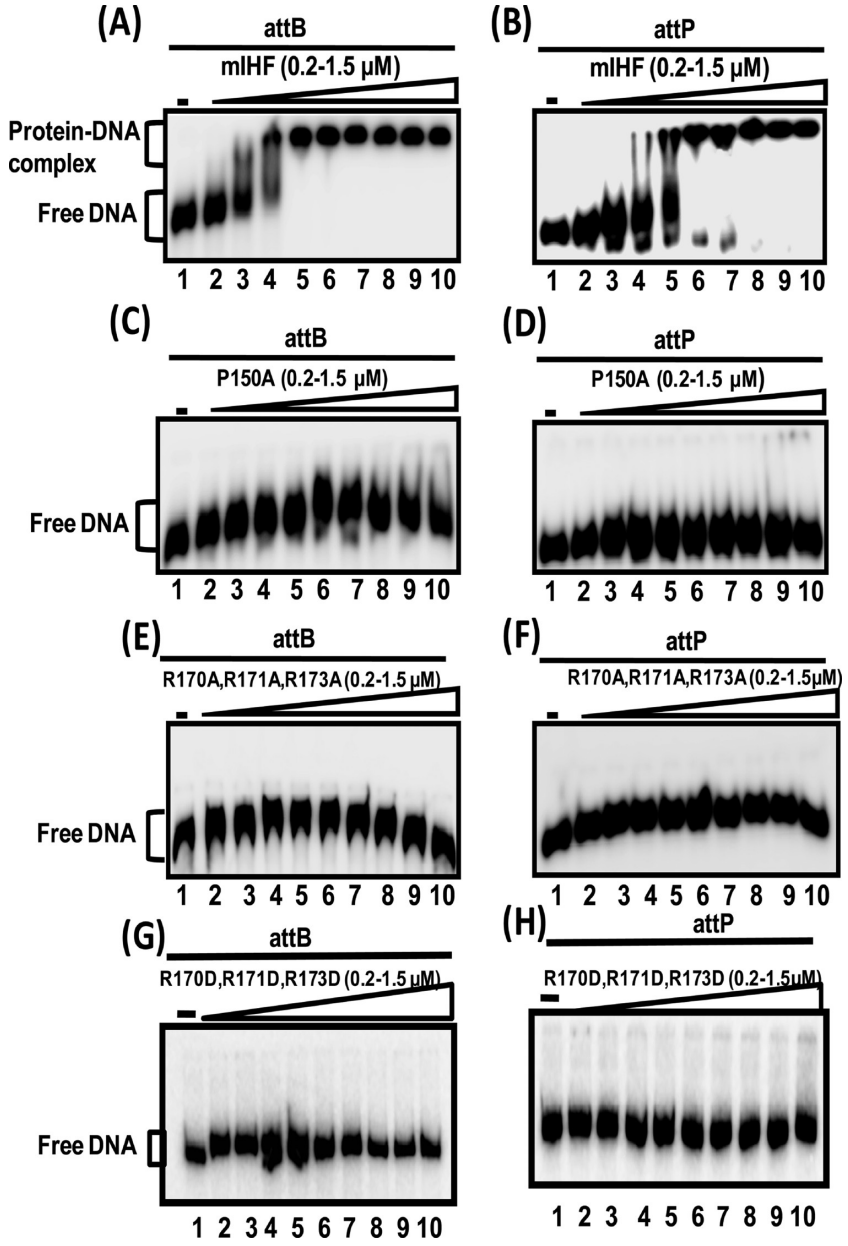

Figure 6. Binding of *M. tuberculosis* wild-type IHF to duplex DNA containing phage L5 *attB* and *attP* sites. The assay was performed as described in Experimental Procedures. Reaction mixtures contained 2 nM ^{32}P-labeled double-stranded DNA bearing *attB* (A, C, E, and G) or *attP* (B, D, F, and H) in the absence (lane 1) or presence of 0.2, 0.3, 0.4, 0.5, 0.6, 0.75, 1, 1.2, and 1.5 μM (lanes 2−10, respectively) wild-type or mutant IHF proteins, respectively. The empty triangle at the top of the gel denotes increasing concentrations of wild-type or mutant IHF proteins.

function of an increasing concentration of mIHF, suggested that mIHF shows an ∼2-fold higher preference for *attB*-containing DNA over *attP* DNA substrate (Figure 7I).

In parallel experiments, we investigated the binding affinity of *E. coli* IHF$\alpha\beta$ for phage L5 *attB*- and *attP*-containing dsDNA. In contrast to mIHF, *E. coli* IHF$\alpha\beta$ bound *attB* DNA at levels equivalent to that of *attP* DNA, but to a lesser extent to curved and noncurved DNA (Figure 8A−D). Furthermore, quantitative analysis of the formation of protein−DNA complexes as a function an increasing concentration of *E. coli* IHF$\alpha\beta$ corroborates the idea that it binds more efficiently to *attB*- and *attP*-containing substrates than to curved and noncurved DNA (Figure 8E).

***M. tuberculosis* IHF Binds with Greater Affinity to Curved DNA, *attP*, and *attB* Than to Noncurved DNA.** A striking feature of *E. coli* IHF$\alpha\beta$ is its ability to bind phage λ *attB* and *attP* sites and induce bends to facilitate the formation of higher-order structures.[8,10,14] *M. smegmatis* IHF appears to promote the integration of phage L5 in a fashion similar to that of *E. coli* IHF$\alpha\beta$.[24,28] To gain further insights into mIHF DNA binding activity, we chose to determine the binding affinity of mIHF for 230 bp curved DNA (derived from plasmid pB16) and 220 bp noncurved dsDNA (derived from plasmid pNB10).[43] The curved DNA is characterized by a high (78%) content of A and T.[43] Binding reactions were performed as described above. We found that mIHF bound with higher affinity to curved dsDNA than to noncurved dsDNA substrate (compare panels A and E of Figure 7). Furthermore, a relatively lower protein concentration of mIHF was required to form complexes with curved DNA than with noncurved DNA.

DOI: 10.1021/acs.biochem.5b00447
Biochemistry 2015, 54, 4142−4160

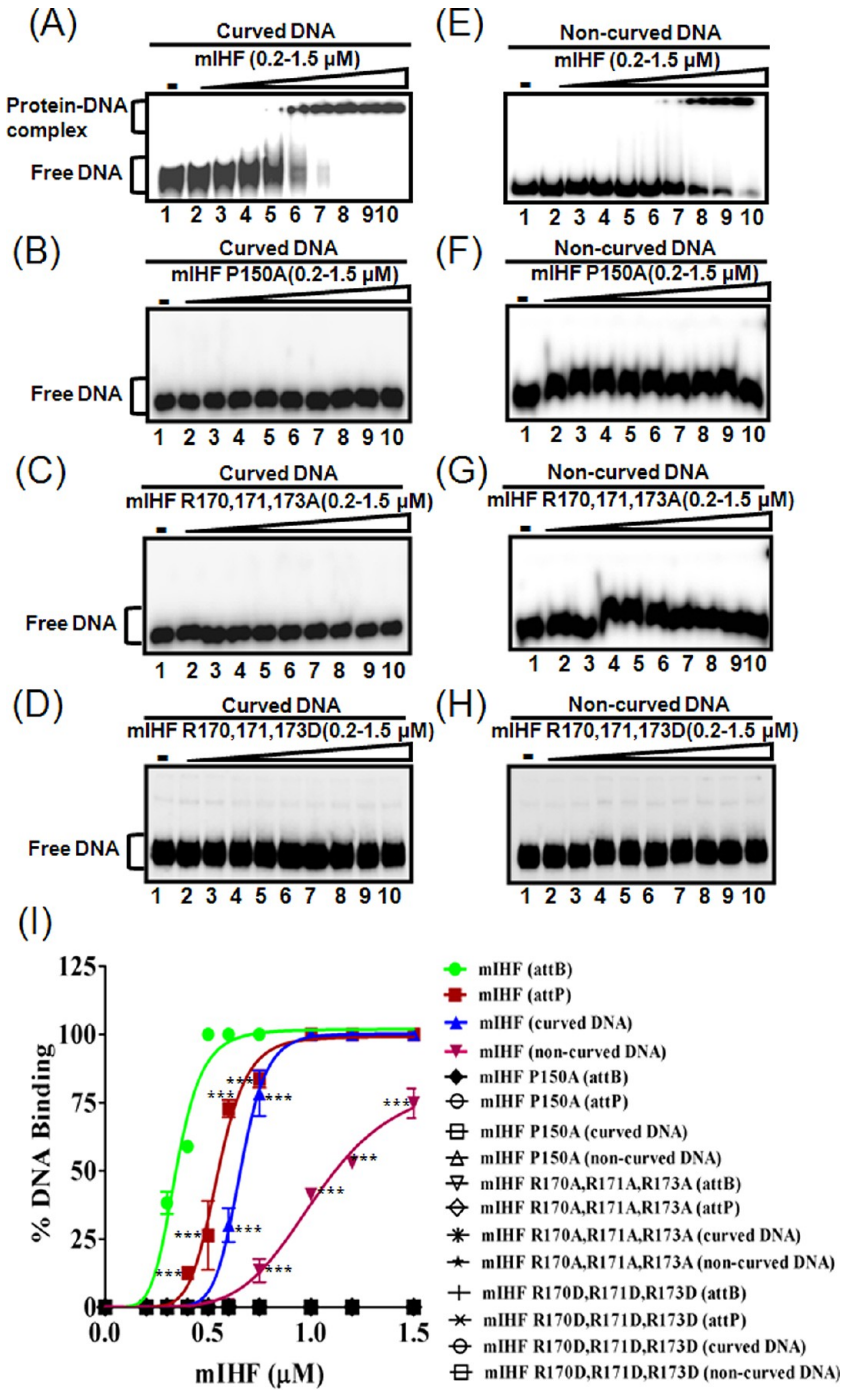

Figure 7. *M. tuberculosis* wild-type IHF shows relatively higher binding affinity for curved DNA. The assay was performed as described in Experimental procedures. Reaction mixtures contained 2 nM ^{32}P-labeled curved (A−D) or noncurved DNA (E−H) in the absence (lane 1) or presence of 0.2, 0.3, 0.4, 0.5, 0.6, 0.75, 1, 1.2, and 1.5 μM mIHF (lanes 2−10, respectively) or its variants (lanes 2−10, respectively). The empty triangle at the top of the gel denotes increasing amounts of wild-type or mutant IHF proteins. (I) Graphical representation showing the extent of binding of various IHF proteins to *attB*, *attP*, curved, and noncurved DNA substrates. Because all the mIHF variants lacked DNA binding activity with each of the substrates tested, the curves representing their binding are merged into the baseline. Statistical analysis was performed using two-way analysis of variance. Data represent means ± the standard deviation from three independent experiments: *P < 0.05, **P < 0.01, and ***P < 0.001 vs mIHF (attB).

Quantitative analysis indicated that the affinity of mIHF for curved DNA is 2-fold higher than for noncurved DNA (Figure 7I and Table 2). Consistent with the data obtained for *attB*- and *attP*-containing DNA substrates, mIHF mutant proteins failed to bind both curved and noncurved DNA even at the highest protein concentrations tested (Figure 7B−D,F−H). Likewise, *E. coli* IHF$\alpha\beta$ displayed a relatively higher binding affinity for curved DNA than for noncurved DNA (Figure 8E).

To ascertain the binding specificity of mIHF for *attP* and *attB* sites, we performed competition experiments using increasing concentrations of noncurved DNA. Figure 9 shows that unlabeled DNA containing *attP* and *attB* sites but not noncurved DNA competed with the formation of ^{32}P-labeled

DOI: 10.1021/acs.biochem.5b00447
Biochemistry 2015, 54, 4142−4160

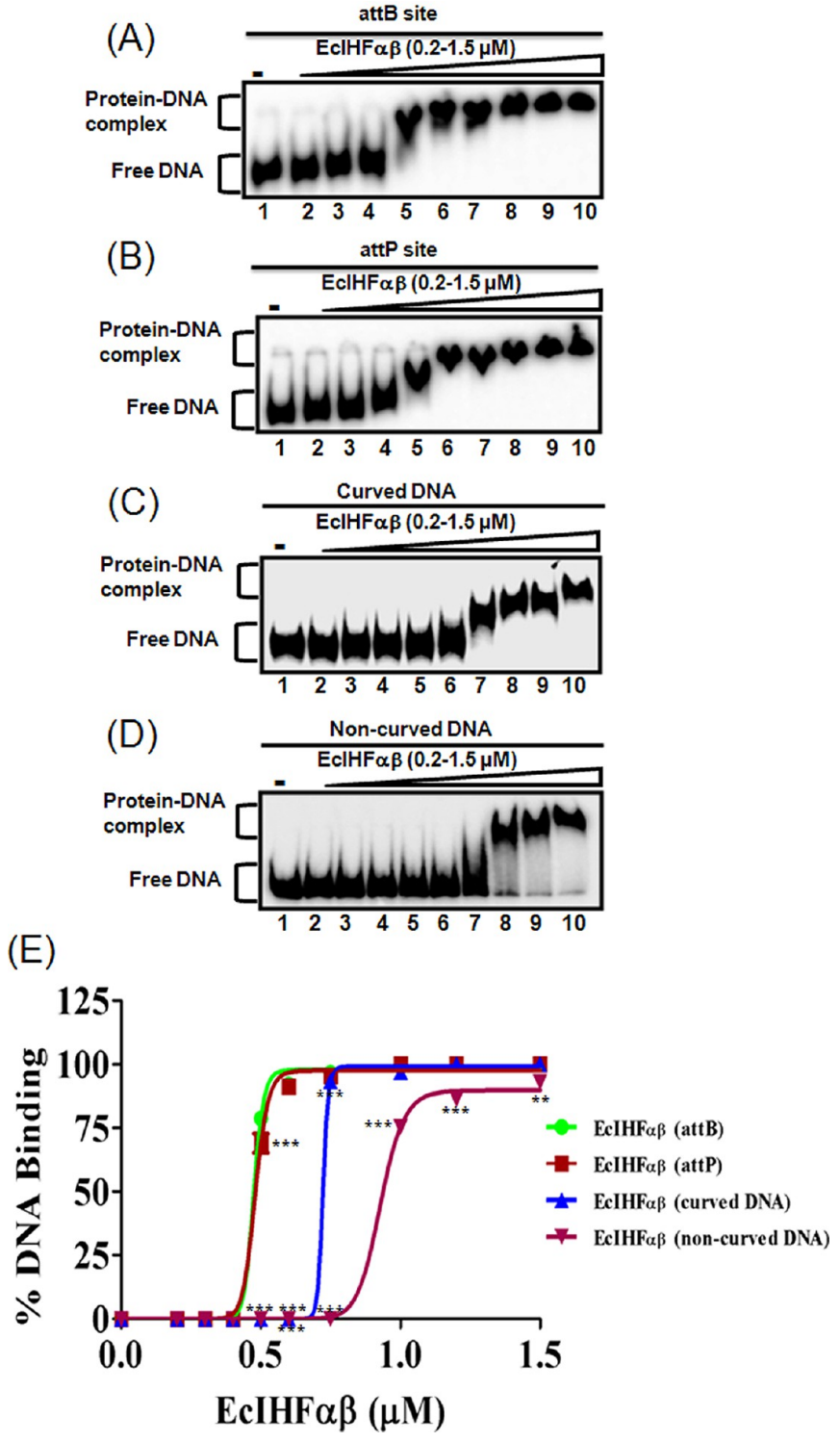

Figure 8. Binding of *E. coli* IHF$\alpha\beta$ to double-stranded DNA containing phage L5 *attB* and *attP* sites as well as curved and noncurved DNA. The assay was performed as described in Experimental Procedures. Reaction mixtures contained 2 nM ^{32}P-labeled *attB* (A), *attP* (B), or curved (C) or noncurved (D) duplex DNA in the absence (lane 1) or presence of 0.2, 0.3, 0.4, 0.5, 0.6, 0.75, 1, 1.2, and 1.5 μM *E. coli* IHF$\alpha\beta$ (lanes 2−10, respectively). The empty triangle at the top of the gel denotes increasing concentrations of *E. coli* IHF$\alpha\beta$. (E) Graphical representation showing the extent of binding of *E. coli* IHF$\alpha\beta$ to DNA containing *attB* and *attP* sites as well as curved and noncurved DNA. Data represent means ± the standard deviation from three independent experiments: $^*P < 0.05$, $^{**}P < 0.01$, and $^{***}P < 0.001$ vs EcIHF$\alpha\beta$ (attB).

DNA−mIHF complexes. To further characterize the binding affinity, we have determined the apparent equilibrium dissociation constant (K_d) of mIHF binding to various DNA substrates in comparison with *E. coli* IHF$\alpha\beta$. The resulting K_d values are summarized in Table 2. We found the K_d values for *attB*- and *attP*-containing fragments to be in the range of 0.3−0.5 μM. These values are similar to those reported for *E. coli* IHF$\alpha\beta$.[56] Although the difference in the affinity between specific and nonspecific DNA is smaller, the weaker binding of IHF proteins to nonspecific DNA is likely to be relevant

DOI: 10.1021/acs.biochem.5b00447
Biochemistry 2015, 54, 4142−4160

Table 2. Dissociation Constants for IHF−DNA Complexes

DNA substrate	K_d (μM)	
	E. coli IHFαβ	mIHF
curved DNA (pB16)	0.60 ± 0.010	0.55 ± 0.012
noncurved DNA (pNB10)	0.90 ± 0.015	1.50 ± 0.010
attP site-containing substrate	0.56 ± 0.012	0.51 ± 0.013
attB site-containing substrate	0.53 ± 0.005	0.30 ± 0.003

because IHF is present at 10−100 μM in the cell (ref 50 and this study).

Binding of mIHF but Not *E. coli* IHFαβ to Phage L5 *attP* and *attB* DNA Produces a Salt-Stable Complex. Elucidation of the thermodynamic parameters of protein−DNA interactions is crucial to the understanding of factors that dictate the function of protein−DNA complexes. The binding affinity and specificity of *E. coli* IHFαβ depend on the salt concentration.[57,58] At low salt concentrations below 100 mM, the specificity of IHF is low and the specificity increases as the salt concentration increases, up to 250 mM. We reasoned that subtle differences between mIHF and *E. coli* IHFαβ in their affinity for dsDNA substrates were not fully pronounced in the assay described above. We therefore investigated the stability of protein−DNA complexes formed by mIHF and *E. coli* IHFαβ in the presence of increasing salt concentrations. Interestingly, even 1.5 M NaCl was not sufficient to dissociate the complexes formed with *attP*- or *attB*-containing DNA by mIHF (Figure 10). On the other hand, complete dissociation of complexes formed by *E. coli* IHFαβ with the same substrates occurred in the presence of 150 mM NaCl (Figure 10). Next we examined the stability of complexes formed by mIHF or *E. coli* IHFαβ with curved and noncurved DNA. The complexes formed with curved DNA remained stable, even in the presence of 1.5 M NaCl (Figure 10). In contrast, the stability of complexes formed by mIHF or *E. coli* IHFαβ with noncurved DNA drastically declined in the presence of 200−300 mM NaCl. The results are summarized in a graphical form in Figure 10I. We observed striking differences in the effect of NaCl on the stability of mIHF−*attB*, mIHF−*attP*, and mIHF−curved DNA complexes compared to those of complexes formed with noncurved DNA. Among the potential explanations for this finding, one possibility is that binding of mIHF to *attP* and *attB* results in encircling of dsDNA, via protein−protein interactions, and hence the establishment of a salt-stable complex. This possibility was supported by the observation that binding of mIHf to curved DNA results in the formation of nucleoid-like structures (see below).

***M. tuberculosis* IHF Mutants Lacking DNA Binding Activity as Well as *E. coli* IHFαβ Fail To Stimulate Site-Specific Recombination Promoted by Phage L5 Integrase.** One of the hallmarks of the IHF family of proteins is their ability to serve as essential cofactors in the integration of phage genome into or excision from the host chromosome. Previous studies have shown that *M. smegmatis* IHF is essential for recombination promoted by phage L5 integrase.[23,28] To further suggest biological significance, we sought to examine the ability of mIHF and its variants to stimulate site-specific recombination as previously described.[28,55] In this assay, recombination between phage L5 *attP* and *attB* sites generates a new DNA species with a molecular weight of ∼8 kb. As shown in Figure 11A, recombination promoted by phage L5 integrase was stimulated by wild-type mIHF in a concentration-dependent manner. In contrast to wild-type mIHF, the Arg to Ala mIHF triple mutant failed to stimulate recombination, even at higher concentrations (Figure 11B). Similar results were obtained in the case of the Arg to Asp mIHF triple mutant (data not shown). As shown above (Figure 3), although the P150A mIHF mutant partially complemented the UV and MMS sensitivity of *E. coli* Δ*ihfA* and Δ*ihfB* strains (Figure 3), the mutant protein failed to form a stable complex with DNA

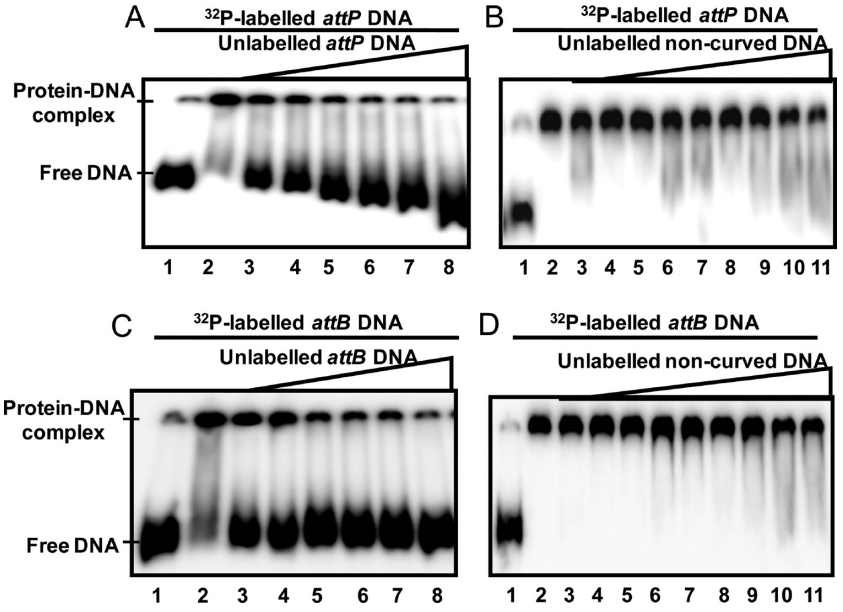

Figure 9. mIHF exhibits a higher affinity for DNA containing *attP* and *attB* sites. The assay was performed as described in Experimental Procedures. Reaction mixtures contained 2 nM ^{32}P-labeled *attB* or *attP* DNA, 1.2 μM mIHF, and increasing concentrations of unlabeled DNA. In all panels, lane 1 contained ^{32}P-labeled substrate and lane 2 the positive control in the absence of competitor DNA. (A and C) In lanes 3−8, the reaction mixture also contained 10, 25, 40, 50, 75, and 100 nM unlabeled competitor DNA, respectively. (B and D) In lanes 3−11, the reaction mixture also contained 5, 10, 15, 25, 30, 40, 50, 75, and 100 nM unlabeled competitor DNA, respectively.

DOI: 10.1021/acs.biochem.5b00447
Biochemistry 2015, 54, 4142−4160

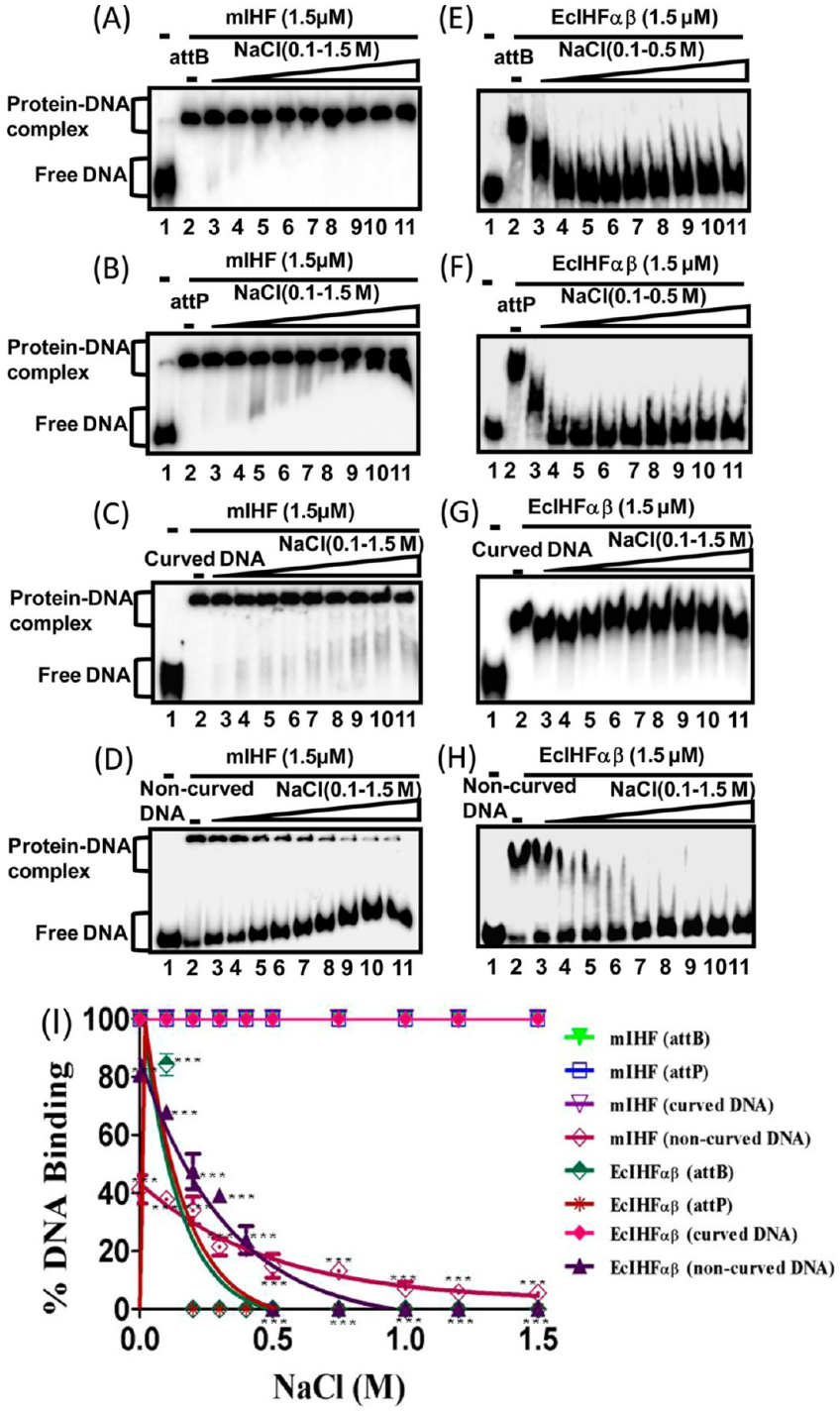

Figure 10. Effect of NaCl on the stability of IHF−DNA complexes. Reaction mixtures contained 2 nM ^{32}P-labeled phage LS *attB* (A and E), *attP* (B and F), curved (C and G), or noncurved (D and H) duplex DNA with 1.5 μM mIHF or *E. coli* IHF$\alpha\beta$. After incubation for 20 min, NaCl was added to final concentrations of 0.1, 0.2, 0.3, 0.4, 0.5, 0.75, 1, and 1.5 M, respectively. After further incubation for 10 min, samples were subjected to electrophoresis on polyacrylamide gels, visualized, and quantitated by phosphorimage analysis. The positions of free DNA and protein−DNA complexes are shown in the left-hand side of each panel. (I) Graphical representation of the extent of dissociation of mIHF−DNA and EcIHF$\alpha\beta$−DNA complexes plotted vs the indicated concentrations of NaCl. Because there was no measurable dissociation of IHF−DNA complexes formed by mIHF with *attB*, *attP*, or curved DNA, and *E. coli* IHF$\alpha\beta$ with curved DNA, the curves are merged and shown at the top of the graph. Statistical analysis of the effect of NaCl on mIHF−DNA complexes. Data represent means ± the standard deviation from three independent experiments: $^{*}P < 0.05$, $^{**}P < 0.01$, and $^{***}P < 0.001$ vs control.

(Figure 6). We reasoned that the P150A mIHF−DNA complex might not be sufficiently stable to persist during an EMSA. Given this scenario, we examined the ability of the P150A mIHF variant to stimulate integrase-promoted recombination. Interestingly, the P150A mutant protein was active and stimulated site-specific recombination, albeit at concentrations somewhat higher than that of wild-type mIHF (Figure 11C). The product formed by P150A was identical to that formed by wild-type mIHF. Next we asked whether a heterologous IHF could stimulate site-specific recombination promoted by phage

DOI: 10.1021/acs.biochem.5b00447
Biochemistry 2015, 54, 4142−4160

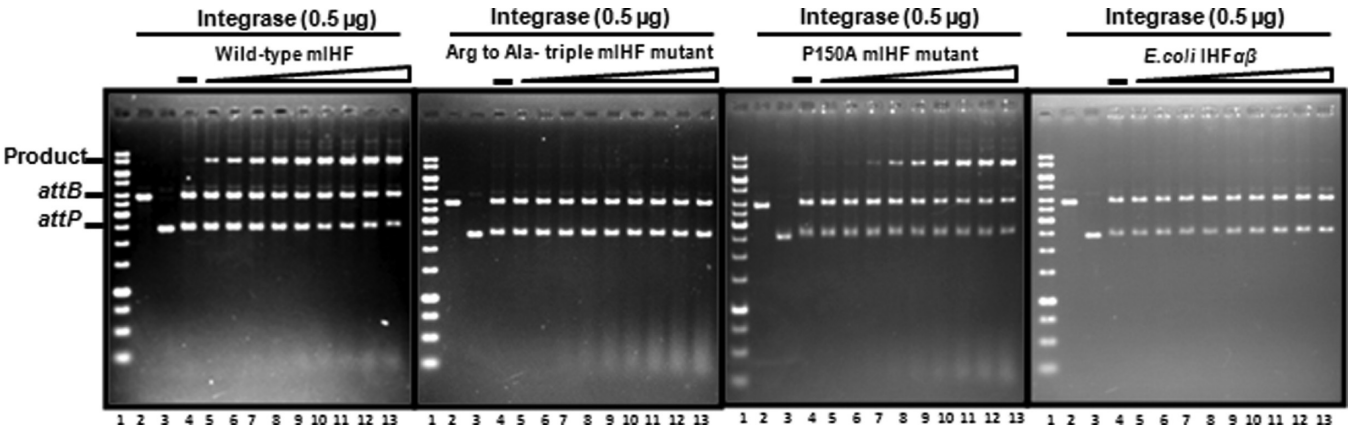

Figure 11. Wild-type mIHF is an essential cofactor for the site-specific recombination reaction promoted by phage L5 integrase between *attB* and *attP* sites. The assay was performed as described in Experimental Procedures. (A) Wild-type mIHF, (B) Arg to Ala triple mutant (R170A/R171A/R173A), (C) P150A mIHF mutant, and (D) *E. coli* IHF$\alpha\beta$: lane 1, DNA markers; lane 2, dsDNA containing the *att*B site; lane 3, negatively supercoiled plasmid DNA containing the *attB* site; lanes 4−13, reaction performed with 0.5 μg of phage L5 integrase and 0.05, 0.1, 0.25, 0.5, 0.75, 1, 1.5, 2, and 2.5 μg of wild-type mIHF, the Arg to Ala triple mutant (R170A/R171A/R173A), or P150A mIHF variants or *E. coli* IHF$\alpha\beta$, respectively. The assays were conducted at least three times for each of the proteins with typical results depicted in panels A−D.

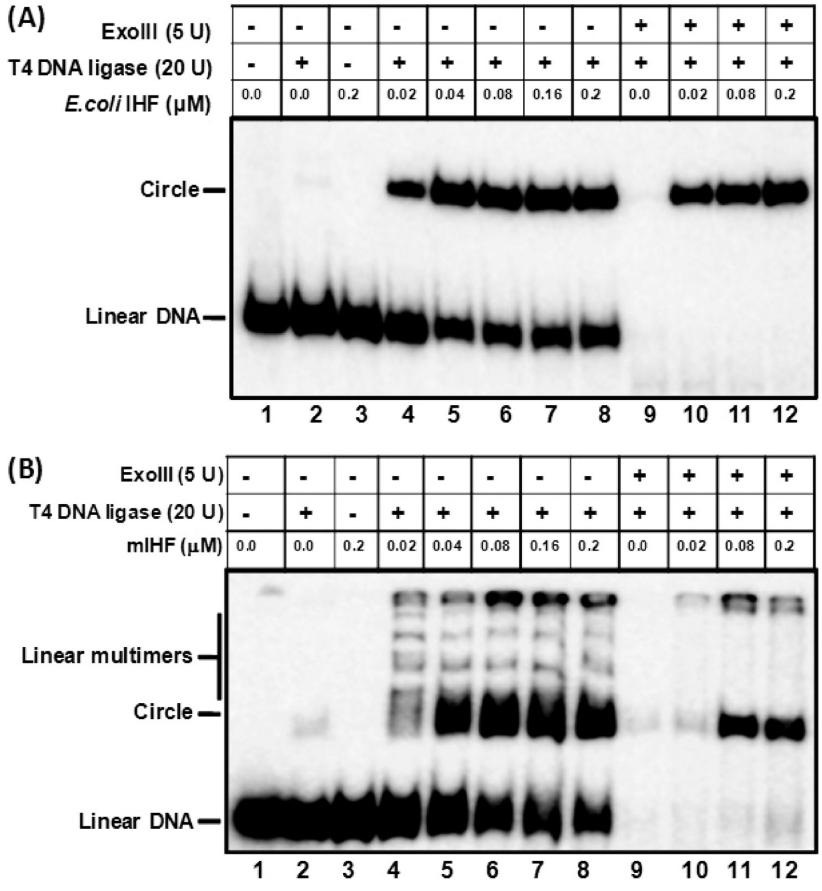

Figure 12. *E. coli* IHF$\alpha\beta$ and mIHF promote the circularization of the 140 bp DNA fragment. The assay was performed as described in Experimental Procedures. (A and B) Reaction mixtures containing 0.25 nM ^{32}P-labeled 140 bp DNA incubated in the absence (lanes 1, 2, and 9) or presence of 20, 40, 80, 160, and 200 nM mIHF (lanes 4−8, respectively). Similar reaction mixtures contained *E. coli* IHF$\alpha\beta$ (lanes 10−12) instead of mIHF and were incubated with 20 units of T4-DNA ligase. In lane 3 of panels A and B, DNA was incubated with 200 nM *E. coli* IHF$\alpha\beta$ or mIHF without ligase. In lanes 9−12, reaction mixtures were incubated with ExoIII, after T4 ligase. The assays were conducted at least three times for each of the proteins with typical results depicted in panels A and B.

L5 integrase. As shown in Figure 11D, *E. coli* IHF$\alpha\beta$ failed to stimulate the reaction. The failure is perhaps due to the inability of *E. coli* IHF$\alpha\beta$ to interact with phage L5 integrase to form a functional intasome.[59] The combined data demonstrate that mIHF is structurally (at the primary and 3D level) and functionally distinct from *E. coli* IHF$\alpha\beta$.

***M. tuberculosis* IHF Promotes Bending of Duplex DNA.** It is known that DNA architectural proteins, such as *E. coli*

DOI: 10.1021/acs.biochem.5b00447
Biochemistry 2015, 54, 4142−4160

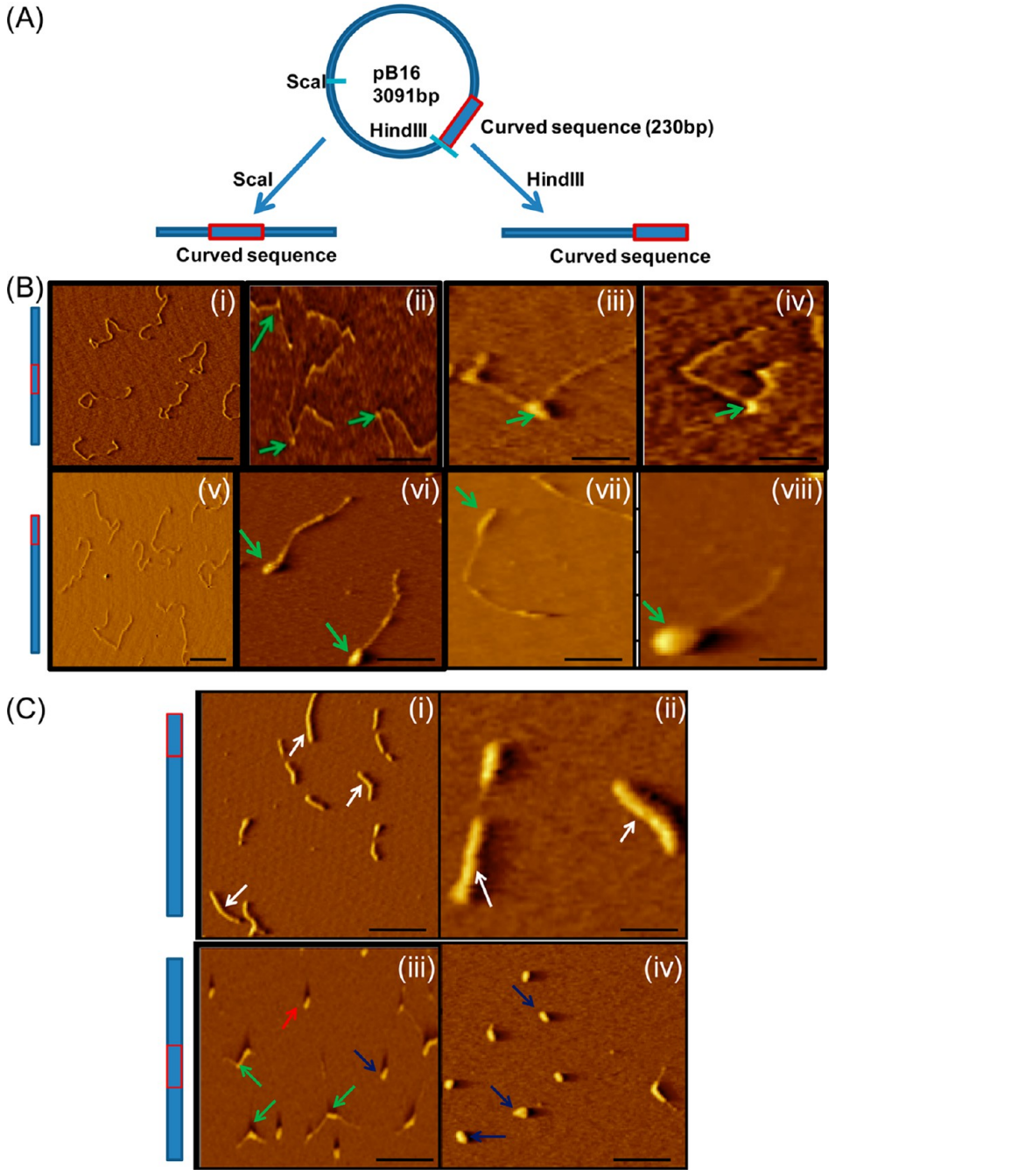

Figure 13. AFM analyses reveal a dual mode of binding of mIHF to DNA. The assay was performed as described inr Experimental Procedures. (A) Schematic diagram showing the preparation of DNA fragments. Part i of panel B and part i of panel C show the representative images of DNA fragments deposited on mica. Parts ii–iv show randomly selected images of mIHF (50 nM) binding to the site embedded at the center of the DNA fragment. In panel B, parts vi–viii show randomly selected images of mIHF (50 nM) binding to the site positioned near the end of the DNA fragment. The green arrow denotes IHF binding. Filled bars on the left-hand side indicate DNA fragments with IHF-binding sites highlighted in red. The scale bars represent 100 nm (B, i and ii), 300 nm (B, ii–iv), and 300 nm (vi–viii). (C) Higher concentrations of mIHF (200 nM) promote the formation of higher-order filamentous and nucleoid-like structures. Parts i and ii show randomly selected images showing the formation of filamentous structures and parts iii and iv randomly selected images depicting the wrapping of DNA into nucleoid-like structures. The filled bars on the left-hand side indicate DNA fragments with an IHF-binding site (red box) at the end or center. A white arrow denotes higher-order filamentous structures; green and blue arrows denote mIHF binding at the center and nucleoid-like structures, respectively. The scale bars represent 300 nm (i, iii, and iv) and 400 nm (ii).

IHF$\alpha\beta$, have the capacity to drastically modify DNA structure by bending.[3] To investigate whether mIHF has the ability to promote DNA bending, we used T4 DNA ligase-catalyzed circularization of the 140 bp DNA fragment excised from pUC19 plasmid DNA, which was devoid of intrinsically bent sequence. The principle underlying this assay is based on the fact that bending of DNA would bring the two ends into the proximity of each other to facilitate ligation. In this assay, we used *E. coli* IHF$\alpha\beta$ as a positive control. We incubated the ^{32}P-labeled DNA fragment first with increasing concentrations of *E.*

DOI: 10.1021/acs.biochem.5b00447
Biochemistry 2015, 54, 4142–4160

coli IHF$\alpha\beta$ or mIHF followed by T4 DNA ligase. Subsequently, reaction mixtures were treated with exonuclease III to remove linear DNA molecules. The DNA products in the reaction mixture were separated by polyacrylamide gel electrophoresis and visualized by phosphorimaging of the dried gels. In the presence of *E. coli* IHF$\alpha\beta$, and in agreement with previous studies,[3,10] we observed the formation of covalently closed circular DNA, which was resistant to exonuclease III digestion (Figure 12A). This species was absent, where ligation was performed in the absence of *E. coli* IHF$\alpha\beta$ (Figure 12A, lane 2). We next examined the ability of mIHF to generate covalently closed DNA molecules. We found that mIHF, over the same range of concentrations, not only exhibited the ability to generate covalently closed DNA molecules but also had the capacity to bridge DNA molecules into linear multimers, albeit to a much lesser extent (Figure 12B, lanes 4−8). We consider that the formation of a linear multimer seen with mIHF posits a role in the overall organization and compactness of the nucleoid.

Different Modes of Binding of mIHF to DNA. A number of studies have shown that *E. coli* IHF$\alpha\beta$ binds with high affinity to a 30−35 bp having a conserved 3′ region with a consensus sequence of WATCAANNNNTTR (where W is A or T, R is purine, and N is any base) and the 5′ region is degenerate but is typically rich in A and T.[8,10,12−14] To gain further insights into the structural features of mIHF−DNA complexes, we generated DNA fragments that had A+T tracts embedded either in the center or near the end (Figure 13A). Reactions were performed under conditions similar to those used for mobility shift assays. The products of the reactions were visualized using atomic force microscopy (AFM). In the absence of mIHF, dsDNA fragments were devoid of bent structures and tangles (Figure 13B, i and v). In reactions performed with DNA fragments containing an A+T tract at the center and limiting amounts of mIHF, we observed that mIHF binding was predominantly at the center so that the two arms extended to either side of the complex (>90%; n = 50) (Figure 13B, ii−iv). Furthermore, this mode of binding resulted in sharp bends around the protein core, and the estimated contour lengths were in agreement with mIHF binding at the center (Figure 13B, ii−iv). Under identical conditions, with a DNA fragment containing and A+T tract near the end, binding was primarily at the ends with no bending (Figure 13B, vi−viii). Interestingly, we observed globular structures at the ends, indicating the formation of higher-order nucleoprotein structures. A further increase in the amount of mIHF led to the formation of two distinct types of structures, one with a DNA fragment having A+T tracts near the end and mIHF first bound to the end and then to the end lacking the A+T tract (n = 52). Subsequently, it spread along the DNA to form rigid nucleoprotein filamentous structures (Figure 13C, i and ii). On the other hand, for DNA fragment that had A-tracts embedded at the center, and mIHF binding resulted in the formation of nucleoid-like structures in which DNA is fully wrapped around the protein core (Figure 13C, iii and iv). The two modes of mIHF binding have important implications for the compaction of DNA into nucleoids and the formation of higher-order nucleoprotein structures.

DISCUSSION

A great deal of structural and biochemical work has been devoted to understanding the functional properties of *E. coli* IHF$\alpha\beta$. Very little is known about the components of nucleoid and their function in mycobacteria, but such knowledge is crucial for understanding the changes that *M. tuberculosis* nucleoid experiences in response to the frequently altering milieu of the host. Multiple-sequence alignment and homology modeling of the mIHF 3D structure indicated that it is unrelated in sequence and structure to the prototype *E. coli* IHF$\alpha\beta$, but similar to that of sIHF (Figure 1). Notwithstanding the structural differences, mIHF alone was necessary and sufficient for the restoration of viability in both *E. coli* Δ*ihfA* and Δ*ihfB* strains against genotoxic stress, could induce DNA compaction, and could catalyze site-specific recombination. The discovery that functionally relevant amino acid residues and the mechanism that governs binding of mIHF to DNA as well as DNA bending are different from those of both *E. coli* IHF$\alpha\beta$ and sIHF, and provide protection from genotoxic stress, is striking. Overall, our data are consistent with the notion that mIHF is a distinct member of the family of proteins that serve as essential cofactors in site-specific recombination and nucleoid organization. Furthermore, we believe that our results represent an important contribution and provide insights into those functions of mIHF that are likely to be essential for the growth and viability of *M. tuberculosis*.

Studies of different bacterial systems have revealed the existence of complexities in the number and intracellular concentrations of NAPs.[1−3] In many bacteria, the intracellular levels of IHF are dependent on the growth conditions, which thereby influences the patterns of gene expression in a temporal fashion.[2,3] Very little is known about the expression patterns and biological significance of NAPs in mycobacteria. Here we show that the expression mIHF follows a dynamic pattern as a function of the growth cycle (Figure 2). Like that of *E. coli* IHF$\alpha\beta$,[3] expression of mIHF manifests during the early exponential phase, and the level of expression increases during the midexponential phase and then reaches plateau during the stationary phase. The growth phenotypes of *E. coli* mutants lacking both IHF and HU are more severe than the phenotypes of single mutants.[52−54] However, it remains possible that IHF mutants may display mild growth attenuation that is not severe enough to be identified in the experiments described in the literature. In contrast to *E. coli*, null mutation of *ihf* in both *M. tuberculosis* and *M. smegmatis* is lethal.[24,28−30] Therefore, we used *E. coli* Δ*ihfA* and Δ*ihfB* strains to explore the biological roles of mIHF under certain stringent environmental conditions. Strikingly, we found that *Mtihf* alone could complement the growth and MMS and UV sensitivity phenotypes of *E. coli* Δ*ihfA* and Δ*ihfB* strains as well as induce DNA compaction, raising the possibility that it may function as a barrier in the defense against genotoxic stress and/or in the regulation of multiple DNA repair pathways.

Our biochemical analyses suggest that wild-type mIHF, in contrast to its mutant variants, binds *attB* and *attP* sites, forms stable nucleoprotein complexes, and stimulates site-specific recombination. Furthermore, by using mutant proteins, we assessed the impact of the amino acid residues identified from our modeling efforts on the biological and biochemical properties of mIHF. We found that the alleles affecting DNA binding failed to complement *E. coli* Δ*ihfA* and Δ*ihfB* strains, and the variant proteins lacked detectable DNA binding activity. Molecular modeling studies showed that the P150 is not in contact with DNA and, therefore, unlikely to be essential for mIHF DNA binding activity. Intriguingly, we found that the P150A mutant protein failed to display significant DNA binding activity as assessed by an EMSA. We speculated that the

DOI: 10.1021/acs.biochem.5b00447
Biochemistry 2015, 54, 4142−4160

inability of the P150 mutant to bind DNA could be due to the instability of the DNA−protein complex during gel mobility assays. This premise is supported by the observation that the P150 mutant protein was able to catalyze site-specific recombination under solution conditions. The similarity in sequence and structure of mIHF and sIHF raises the question of how these two closely related proteins perform their functions with requirements for binding specificity. While mIHF can bind nonspecific sequences, it forms especially "stable" high-affinity complexes with cognate DNA that are not disrupted by the addition of a high salt concentration and competitor DNA. On the other hand, sIHF interacts nonspecifically with double-stranded DNA with a K_d in the micromolar range.[48] The ability to interact with cognate DNA as well as nonspecific sequences at varying affinities is a common characteristic of the IHF-HU DNABII superfamily of proteins.[3,8,10] In the cocrystal structure of sIHF with 19 bp DNA, the interface between sIHF and DNA is less extensive and showed no significant DNA bending.[48] Although the amino acid residues of sIHF involved in DNA binding have not been identified, it is devoid of the conserved proline residue present in *E. coli* IHF that becomes inserted into the minor groove and introduces DNA bends.[8] However, the lack of DNA bending in the cocrystal structure of the sIHF−DNA complex may not be due to lack of proline, but possibly due to a short stretch of duplex DNA.

Our studies reveal that mIHF causes wrapping and bending of short DNA fragments, suggesting a probable mechanism underlying the formation of nucleoid-like structures. By analyzing both target and nontarget DNA substrates, we observed that mIHF displays a relatively higher affinity for phage L5 *attP* and *attB* sites and DNA rich in A/T sequences. These findings are in agreement with those of earlier studies of *E. coli* IHF$\alpha\beta$.[10,12,13,60,61] Comparison of more than 170 known *E. coli* IHF$\alpha\beta$-binding sites has led to the identification of a consensus DNA-binding motif.[10,61,62] Among these, the two most highly conserved elements are the WATCAA sequence starting near the center of the site and the second sequence TTR located 4 bp in the 3′ direction from the WATCAA sequence.[61−63] Other high-affinity binding sites of *E. coli* IHF$\alpha\beta$ contain a poly(A) tract containing four to six adenines.[64,65] Although mIHF exhibits a relatively high affinity for phage L5 *attP* and *attB* sites, further studies are necessary to identify the consensus binding motif(s) in these sites. Since its discovery,[4] *E. coli* IHF$\alpha\beta$ has attracted considerable attention because of its role in various DNA transactions, wherein IHF-induced sharp bends or DNA loops coordinate the cooperative assembly of multicomponent nucleoprotein complexes.[2,3,8] The biochemical data, combined with the crystal structures, have shown that *E. coli* IHF$\alpha\beta$ binds to the minor groove of DNA and bends the double helix by >160°.[14,66,67] Other studies have shown that binding of *E. coli* IHF$\alpha\beta$ to DNA and subsequently DNA bending occur in a concerted fashion.[66−68]

Nucleoid-associated proteins are bifunctional molecular entities. First, the ensemble and single-molecule measurements have shown that NAPs contribute to DNA architecture in the organization of bacterial chromatin by folding and packaging of DNA into nucleoids. Second, NAPs play key roles in the regulation of many important genes by interaction with specific sequences in the target gene promoters. One of the traditional views with regard to roles of NAPs is that, because of their high abundance and promiscuity with respect to DNA binding, they play key roles in the regulation of transcription by modulating the state of DNA structure.[1−3] An array of mechanisms has been described by which NAPs mediate compaction of DNA into nucleoids and regulate gene expression. As the affinity of NAPs for DNA is generally weak, cooperative binding is essential to increase the local concentrations of NAPs near the target sites. Other mechanisms include introduction and constraining of DNA supercoiling and bridging of adjacent segments of DNA. Collectively, these processes are thought to influence the gene order along the genome and likely regulate the temporal order of gene expression.[1−3] Despite these advances, our knowledge with respect to the factors and the molecular mechanism that determine the choice between the architectural and regulatory roles of NAPs remains poorly understood. Our study provides insights into the determinants involved in the formation of filamentous and nucleoid-like structures. Altogether, our findings are consistent with the notion that the dual roles of IHF may be determined by its binding position relative to the genes it controls.

While considering the capacity of mIHF to engage in genome organization and as a global transcriptional silencer, it is useful to understand its physical impact on the DNA to which it binds. Our study suggests that the sequence determinants and their context might influence the choice between the processes mentioned above. We also note that this is a fundamental mechanism pertinent to nucleoid organization and gene expression, which may be generally applicable to all the IHF-regulated genes and binding sites in bacterial cells.[69] Given the fact that sIHF and mIHF are structurally related, interestingly, sIHF is not essential for growth but is required for normal chromosome compaction.[48] On the other hand, because IHF is essential for *M. tuberculosis* growth, it is likely to be involved in multiple essential biological functions as well as in the maintenance of genome integrity; as such, this can be exploited in drug screening efforts.

AUTHOR INFORMATION

Corresponding Author

*E-mail: kmbc@biochem.iisc.ernet.in. Telephone: (91-80) 2293 2235/2360 0278. Fax: (91-80) 2360 0814/0683.

Author Contributions

N.S. and Y.H. contributed equally to this work.

Funding

This work was supported by grants from the Department of Biotechnology under the Center of Excellence and Innovation in Biotechnology program, New Delhi, and a J. C. Bose National Fellowship from the Department of Science and Technology, New Delhi, to K.M.

Notes

The authors declare no competing financial interest.

ACKNOWLEDGMENTS

We are indebted to Graham Hatfull, Claudio Gualerzi, and Jim Maher III for their kind gift of plasmids and *E. coli* strains, Usha Karthikeyan for her assistance with AFM, Dibyendu Bhattacharya for 3D image reconstruction, and B. Gopal for anti-SigA antibodies.

ABBREVIATIONS

AFM, atomic force microscopy; BPB, bromophenol blue; BSA, bovine serum albumin; DAPI, 4′,6-diamidino-2-phenylindole; dsDNA, double-stranded DNA; DTT, dithiothreitol; EDTA, ethylenediaminetetraacetic acid; EMSA, electrophoretic mobi-

DOI: 10.1021/acs.biochem.5b00447
Biochemistry 2015, 54, 4142−4160

lity shift assay; IPTG, isopropyl β-D-thiogalactopyranoside; mIHF, *M. tuberculosis* IHF; MMS, methylmethanesulfonate; NAP, nucleoid-associated proteins; PAGE, polyacrylamide gel electrophoresis; PBS, phosphate-buffered saline; SDS, sodium dodecyl sulfate.

REFERENCES

(1) Travers, A., and Muskhelishvili, G. (2005) Bacterial chromatin. *Curr. Opin. Genet. Dev. 15*, 507−514.

(2) Dame, R. T. (2005) The role of nucleoid-associated proteins in the organization and compaction of bacterial chromatin. *Mol. Microbiol. 56*, 858−870.

(3) Dorman, C. J. (2013) Genome architecture and global gene regulation in bacteria: Making progress towards a unified model? *Nat. Rev. Microbiol. 11*, 349−355.

(4) Williams, J. G. K., Wulff, D. L., and Nash, H. A. (1977) A mutant of *Escherichia coli* deficient in a host function required for phage lambda integration and excision. In *DNA insertion elements, plasmids and episomes* (Bukhari, A., Shapiro, J., and Adhya, S., Eds.) pp 357−361, Cold Spring Harbor Laboratory Press, Plainview, NY.

(5) Rouviere-Yaniv, J., and Gros, F. (1975) Characterization of a novel, low-molecular-weight DNA-binding protein from *Escherichia coli*. *Proc. Natl. Acad. Sci. U.S.A. 72*, 3428−3432.

(6) Peacock, S., Weissbach, H., and Nash, H. A. (1984) *In vitro* regulation of phage λ cII gene expression by *E. coli* integration host factor. *Proc. Natl. Acad. Sci. U.S.A. 81*, 6009−6013.

(7) Browning, D. F., Cole, J. A., and Busby, S. J. W. (2008) Regulation by nucleoid-associated proteins at the *Escherichia coli* nir operon promoter. *J. Bacteriol. 190*, 7258−7267.

(8) Swinger, K. K., and Rice, P. A. (2004) IHF and HU: Flexible architects of bent DNA. *Curr. Opin. Struct. Biol. 14*, 28−35.

(9) Bertoni, G., Fujita, N., Ishihama, A., and de Lorenzo, V. (1998) Active recruitment of σ54-RNA polymerase to the Pu promoter of *Pseudomonas putida*: Role of IHF and αCTD. *EMBO J. 17*, 5120−5128.

(10) Landy, A. (1989) Dynamic, structural and regulatory aspects of λ site specific recombination. *Annu. Rev. Biochem. 38*, 913−949.

(11) Justice, S. S., Li, B., Downey, J. S., Dabdoub, S. M., Brockson, M. E., Probst, G. D., Ray, W. C., and Goodman, S. D. (2012) Aberrant community architecture and attenuated persistence of uropathogenic *Escherichia coli* in the absence of individual IHF subunits. *PLoS One 7* (10), e48349.

(12) Craig, N. L., and Nash, H. A. (1984) *E. coli* integration host factor binds to specific sites in DNA. *Cell 39*, 707−716.

(13) Yang, C. C., and Nash, H. A. (1989) The interaction of *E. coli* IHF protein with its specific binding sites. *Cell 57*, 869−880.

(14) Rice, P. A., Yang, S., Mizuuchi, K., and Nash, H. A. (1996) Crystal structure of an IHF-DNA complex: A protein-induced DNA U-turn. *Cell 87*, 1295−1306.

(15) Lin, J., Chen, H., Dröge, P., and Yan, J. (2012) Physical organization of DNA by multiple non-specific DNA-binding modes of integration host factor (IHF). *PLoS One 7* (11), e49885.

(16) Le, S., Chen, H., Cong, P., Lin, J., Dröge, P., and Yan, J. (2013) Mechanosensing of DNA bending in a single specific protein-DNA complex. *Sci. Rep. 3*, 3508.

(17) Browning, D. F., Grainger, D. C., and Busby, S. J. W. (2010) Effects of nucleoid-associated proteins on bacterial chromosome structure and gene expression. *Curr. Opin. Microbiol. 13*, 773−780.

(18) Arfin, S. M., Long, A. D., Ito, E. T., Tolleri, L., Riehle, M. M., Paegle, E. S., and Hatfield, G. W. (2000) Global gene expression profiling in *Escherichia coli* K12. The effects of integration host factor. *J. Biol. Chem. 275*, 29672−29684.

(19) Dorman, C. J., and Higgins, C. F. (1987) Fimbrial phase variation in *Escherichia coli*: Dependence on integration host factor and homologies with other site-specific recombinases. *J. Bacteriol. 169*, 3840−3843.

(20) Mangan, M. W., Lucchini, S., Danino, V., Croinin, T. O., Hinton, J. C., and Dorman, C. J. (2006) The integration host factor (IHF) integrates stationary-phase and virulence gene expression in *Salmonella enterica serovar Typhimurium*. *Mol. Microbiol. 59*, 1831−1847.

(21) Stonehouse, E., Kovacikova, G., Taylor, R. K., and Skorupski, K. (2008) Integration host factor positively regulates virulence gene expression in *Vibrio cholerae*. *J. Bacteriol. 190*, 4736−4748.

(22) Corcoran, C. P., and Dorman, C. J. (2009) DNA relaxation-dependent phase biasing of the *fim* genetic switch in *Escherichia coli* depends on the interplay of H-NS, IHF and LRP. *Mol. Microbiol. 74*, 1071−1082.

(23) Lee, M. H., and Hatfull, G. (1993) Mycobacteriophage L5 integrase-mediated site-specific integration in vitro. *J. Bacteriol. 175*, 6836−6841.

(24) Pedulla, M. L., Lee, M. H., Lever, D. C., and Hatfull, G. F. (1996) A novel host factor for integration of mycobacteriophage L5. *Proc. Natl. Acad. Sci. U.S.A. 93*, 15411−15416.

(25) Cole, S. T., Brosch, R., Parkhill, J., Garnier, T., Churcher, C., Harris, D., Gordon, S. V., Eiglmeier, K., Gas, S., Barry, C. E., III, et al. (1998) Deciphering the biology of *Mycobacterium tuberculosis* from the complete genome sequence. *Nature 393*, 537−544.

(26) Sharadamma, N., Harshavardhana, Y., Singh, P., and Muniyappa, K. (2010) *Mycobacterium tuberculosis* nucleoid-associated DNA-binding protein H-NS binds with high-affinity to the Holliday junction and inhibits strand exchange promoted by RecA protein. *Nucleic Acids Res. 38*, 3555−3569.

(27) Sharadamma, N., Khan, K., Kumar, S., Patil, K. N., Hasnain, S. E., and Muniyappa, K. (2011) Synergy between the N- and C-terminal domains of *Mycobacterium tuberculosis* HupB is essential for high-affinity binding, DNA supercoiling and inhibition of RecA-promoted strand exchange. *FEBS J. 278*, 3447−3462.

(28) Pedulla, M. L., and Hatfull, G. F. (1998) Characterization of the mIHF gene of *Mycobacterium smegmatis*. *J. Bacteriol. 180*, 5473−5477.

(29) Sassetti, C. M., and Rubin, E. J. (2003) Genetic requirements for mycobacterial survival during infection. *Proc. Natl. Acad. Sci. U.S.A. 100*, 12989−12994.

(30) Sassetti, C. M., Boyd, D. H., and Rubin, E. J. (2003) Genes required for mycobacterial growth defined by high density mutagenesis. *Mol. Microbiol. 48*, 77−84.

(31) Apweiler, R., Bairoch, A., Wu, C. H., Barker, W. C., Boeckmann, B., Ferro, S., Gasteiger, E., Huang, H., Lopez, R., Magrane, M., Martin, M. J., Natale, D. A., O'Donovan, C., Redaschi, N., and Yeh, L. S. (2004) UniProt: The Universal Protein knowledgebase. *Nucleic Acids Res. 32*, D115−D119.

(32) Berman, H. M., Westbrook, J., Feng, Z., Gilliland, G., Bhat, T. N., Weissig, H., Shindyalov, I. N., and Bourne, P. E. (2000) The Protein Data Bank. *Nucleic Acids Res. 28*, 235−242.

(33) Altschul, S. F., Madden, T. L., Schäffer, A. A., Zhang, J., Zhang, Z., Miller, W., and Lipman, D. J. (1997) Gapped BLAST and PSI-BLAST: A new generation of protein database search programs. *Nucleic Acids Res. 25*, 3389−3402.

(34) Eswar, N., Eramian, D., Webb, B., Shen, M. Y., and Sali, A. (2008) Protein structure modeling with MODELLER. *Methods Mol. Biol. 426*, 145−159.

(35) Pei, J., Kim, B. H., and Grishin, N. V. (2008) PROMALS3D: A tool for multiple protein sequence and structure alignments. *Nucleic Acids Res. 36*, 2295−2300.

(36) McGuffin, L. J., Bryson, K., and Jones, D. T. (2000) The PSIPRED protein structure prediction server. *Bioinformatics 16*, 404−405.

(37) Rodrigues, J. P., Levitt, M., and Chopra, G. (2012) KoBaMIN: A knowledge-based minimization web server for protein structure refinement. *Nucleic Acids Res. 40*, W323−W328.

(38) Shen, M. Y., and Sali, A. (2006) Statistical potential for assessment and prediction of protein structures. *Protein Sci. 15*, 2507−2524.

(39) Jo, S., Vargyas, M., Vasko-Szedlar, J., Roux, B., and Im, W. (2008) PBEQ-Solver for online visualization of electrostatic potential of biomolecules. *Nucleic Acids Res. 36*, W270−W275.

DOI: 10.1021/acs.biochem.5b00447
Biochemistry 2015, 54, 4142−4160

(40) Sambrook, J., Fritsch, E. F., and Maniatis, T. (1989) *Molecular Cloning: A Laboratory Manual*, 2nd ed., Cold Spring Harbor Laboratory Press, Plainview, NY.
(41) Jacobs, W. R., Jr., Kalpana, G. V., Cirillo, J. D., Pascopella, L., Snapper, S. B., Udani, R. A., Jones, W., Barletta, R. G., and Bloom, B. R. (1991) Genetic systems for mycobacteria. *Methods Enzymol. 204*, 537−555.
(42) Thakur, R. S., Basavaraju, S., Somyajit, K., Jain, A., Subramanya, S., Muniyappa, K., and Nagaraju, G. (2013) Evidence for the role of *Mycobacterium tuberculosis* RecG helicase in DNA repair and recombination. *FEBS J. 280*, 1841−1860.
(43) Spurio, R., Falconi, M., Brandi, A., Pon, C. L., and Gualerzi, C. O. (1997) The oligomeric structure of nucleoid protein H-NS is necessary for recognition of intrinsically curved DNA and for DNA bending. *EMBO J. 16*, 1795−1805.
(44) Lynch, T. W., Read, E. K., Mattis, A. N., Gardner, J. F., and Rice, P. A. (2003) Integration host factor: Putting a twist on protein-DNA recognition. *J. Mol. Biol. 30*, 493−502.
(45) Bhave, M., Papanikou, E., Iyer, P., Pandya, K., Jain, B. K., Ganguly, A., Sharma, C., Pawar, K., Austin, J., II, Day, K. J., Rossanese, O. W., Glick, B. S., and Bhattacharyya, D. (2014) Golgi enlargement in Arf-depleted yeast cells is due to altered dynamics of cisternal maturation. *J. Cell Sci. 127*, 250−257.
(46) Lewis, J. A., and Hatfull, G. F. (2000) Identification and characterization of mycobacteriophage L5 excisionase. *Mol. Microbiol. 35*, 350−360.
(47) Khan, K., Karthikeyan, U., Li, Y., Yan, J., and Muniyappa, K. (2012) Single-molecule DNA analysis reveals that yeast Hop1 protein promotes DNA folding and synapsis: Implications for condensation of meiotic chromosomes. *ACS Nano 6*, 10658−10666.
(48) Swiercz, J. P., Nanji, T., Gloyd, M., Guarne, A., and Elliot, M. A. (2013) A novel nucleoid-associated protein specific to the actinobacteria. *Nucleic Acids Res. 41*, 4171−4184.
(49) Ashkenazy, H., Erez, E., Martz, E., Pupko, T., and Ben-Tal, N. (2010) ConSurf 2010: Calculating evolutionary conservation in sequence and structure of proteins and nucleic acids. *Nucleic Acids Res. 38* (Web Server issue), W529−W533.
(50) Ali, A. T., Iwata, A., Nishimura, A., Ueda, S., and Ishihama, A. (1999) Growth phase-dependent variation in protein composition of the *Escherichia coli* nucleoid. *J. Bacteriol. 181*, 6361−6370.
(51) Gautam, U. S., Sikri, K., Vashist, A., Singh, V., and Tyagi, J. S. (2014) Essentiality of DevR/DosR interaction with SigA for the dormancy survival program in *Mycobacterium tuberculosis*. *J. Bacteriol. 196*, 790−799.
(52) Kano, Y., and Imamoto, F. (1990) Requirement of integration host factor (IHF) for growth of *Escherichia coli* deficient in HU protein. *Gene 89*, 133−137.
(53) Yasuzawa, K., Hayashi, N., Goshima, N., Kohno, N. K., Imamoto, F., and Kano, Y. (1992) Histone-like proteins are required for cell growth and constraint of supercoils in DNA. *Gene 122*, 9−15.
(54) Friedman, D. I. (1988) Integration host factor: A protein for all reasons. *Cell 55*, 545−554.
(55) Singh, S., Plaks, J. G., Homa, N. J., Amrich, C. G., Héroux, A., Hatfull, G. F., and VanDemark, A. P. (2014) The structure of Xis reveals the basis for filament formation and insight into DNA bending within a mycobacteriophage intasome. *J. Mol. Biol. 426*, 412−422.
(56) Yang, S. W., and Nash, H. A. (1995) Comparison of protein binding to DNA in vivo and in vitro: Defining an effective intracellular target. *EMBO J. 14*, 6292−6300.
(57) Holbrook, J. A., Tsodikov, O. V., Saecker, R. M., and Record, M. T., Jr. (2001) Specific and non-specific interactions of integration host factor with DNA: Thermodynamic evidence for disruption of multiple IHF surface salt-bridges coupled to DNA binding. *J. Mol. Biol. 310*, 379−401.
(58) Vitko, J., Rujan, I., Androga, L., Mukerji, I., and Bolton, P. H. (2007) Molecular beacon-equilibrium cyclization detection of DNA-protein complexes. *Biophys. J. 93*, 3210−3217.
(59) Peña, C. E., Kahlenberg, J. M., and Hatfull, G. F. (1999) Protein-DNA complexes in mycobacteriophage L5 integrative recombination. *J. Bacteriol. 181*, 454−461.
(60) Goodman, S. D., Velten, N. J., Gao, Q., Robinson, S., and Segall, A. M. (1999) *In vitro* selection of integration host factor binding sites. *J. Bacteriol. 181*, 3246−3255.
(61) Aeling, K. A., Opel, M. L., Steffen, N. R., Tretyachenko-Ladokhina, V., Hatfield, G. W., Lathrop, R. H., and Senear, D. F. (2006) Indirect recognition in sequence-specific DNA binding by *Escherichia coli* integration host factor: The role of DNA deformation energy. *J. Biol. Chem. 281*, 39236−39248.
(62) Goodrich, J. A., Schwartz, M. L., and McClure, W. R. (1990) Searching for and predicting the activity of sites for DNA binding proteins: Compilation and analysis of the binding sites for *Escherichia coli* integration host factor (IHF). *Nucleic Acids Res. 18*, 4993−5000.
(63) Engelhorn, M., Boccard, F., Murtin, C., Prentki, P., and Geiselmann, J. (1995) In vivo interaction of the *Escherichia coli* integration host factor with its specific binding sites. *Nucleic Acids Res. 23*, 2959−2965.
(64) Hales, L. M., Gumport, R. I., and Gardner, J. F. (1996) Examining the contribution of a dA+dT element to the conformation of *Escherichia coli* integration host factor-DNA complexes. *Nucleic Acids Res. 24*, 1780−1786.
(65) Hales, L. M., Gumport, R. I., and Gardner, J. F. (1994) Determining the DNA sequence elements required for binding integration host factor to two different target sites. *J. Bacteriol. 176*, 2999−3006.
(66) Lorenz, M., Hillisch, A., Goodman, S. D., and Diekmann, S. (1999) Global structure similarities of intact and nicked DNA complexed with IHF measured in solution by fluorescence resonance energy transfer. *Nucleic Acids Res. 27*, 4619−4625.
(67) Vivas, P., Velmurugu, Y., Kuznetsov, S. V., Rice, P. A., and Ansari, A. (2012) Mapping the transition state for DNA bending by IHF. *J. Mol. Biol. 418*, 300−315.
(68) Dhavan, G. M., Crothers, D. M., Chance, M. R., and Brenowitz, M. (2002) Concerted binding and bending of DNA by *Escherichia coli* integration host factor. *J. Mol. Biol. 315*, 1027−1037.
(69) Ishihama, A. (2010) Prokaryotic genome regulation: Multifactor promoters, multitarget regulators and hierarchic networks. *FEMS Microbiol. Rev. 34*, 628−645.

DOI: 10.1021/acs.biochem.5b00447
Biochemistry 2015, 54, 4142−4160